Project Report

Exploring Superconducting Quantum Circuits

Guide: Prof. Vibhor Singh
Indian Institute of Science, Bengaluru

A R Bathri Narayanan
Roll no: P0211501
UM DAE Centre for Excellence in Basic Sciences

Report presented for the
Physics Project Course (PPr 901)

School of Physical Sciences
UM-DAE Centre for Excellence in Basic Sciences
Mumbai, MH, India

Certificate

This is to certify that A R Bathri Narayanan, student of UM DAE CEBS, has undertaken project work from 1st June, 2025 to 29th November, 2025 under the guidance of Prof. Vibhor Singh, Indian Institute of Science, Bengaluru.

This submitted report titled Exploring Superconducting Quantum Circuits is towards the academic requirements of the Integrated Msc. course at UM DAE CEBS.

A. R Bathri Narayanan
29/11/2025

Signature of Student
A R Bathri Narayanan
UM DAE CEBS

Signature of Guide
Prof. Vibhor Singh
Indian Institute of Science, Bengaluru

School of Physical Sciences
Centre for Excellence in Basic Sciences
Mumbai - 400098

Declaration

I declare that this written submission represents my ideas in my own words and where others ideas or works have have been included, I have adequately cited and referenced the original sources. I also declare that I have adhered to all principles of academic honesty and integrity while not having misrepresented, fabricated or falsified any idea/data/fact/source in my submission. I understand that any violation of the above will be cause for disciplinary action by the institute and can also evoke penal action from the sources which have thus not been properly cited or from whom proper permission has not been taken when required.

A. R Bathri Narayanan
29/11/2025

Signature of Student
A R Bathri Narayanan
UM DAE CEBS

Acknowledgments

The six months of my Master's thesis period taught me a lot of things, both academically and non academically.

First, I would like to thank Prof. Vibhor Singh for providing me with an opportunity to work in his lab. He has been very approachable and helpful, giving me new ideas and helping me whenever I got stuck somewhere.

I would like to thank Prof. Vibhor's group (Aman Tyagi, Mridul Kandpal, Anshika Ranjan, Sayani Pal, Mousumi Haldar, Keerthan, Moulik, Sindhu Gnanam, Satyarth Srivastava) for helping me whenever required. I would like to thank Aman for getting me started during the initial days, giving me adequate resources, training, and motivation.

I also take a moment to thank the Indian Institute of Science for hosting me and providing facilities such as access to articles, software, and the canteen. I thank Top 10 Grand PG, Mathikere, and the manager, Mr. Shyam for providing accommodation and the required facilities. I would like to thank my roommate Vishal Nair for bearing with my sleepless nights.

I would like to thank my cousins Abhishek, Sowmya Abhishek and MM Sandhya for making my Bengaluru stay comfortable and memorable. I am also grateful to Bengaluru Bookies (especially Sowmya Ramesh, Kavya Digge, Sanjay Manasali, and Vishal Manasali to name a few of the many friends I had made) for making my weekends special and patiently listening to my ideas.

I finally thank my family for financial and moral support.

SYNOPSIS

Name: A R Bathri Narayanan

Course: Integrated M.Sc in Physics, UM DAE Centre for Excellence in Basic Sciences, Mumbai

Title: Exploring Superconducting Quantum Circuits

Thesis supervisor: Prof. Vibhor Singh

Affiliation: Indian Institute of Science, Bengaluru

ABSTRACT

This thesis presents an understanding of analytical and numerical tools for understanding and modeling superconducting circuits. To understand the prerequisites and working of these tools, we first examine the Duffing oscillator as an introductory nonlinear system, finding its amplitude–frequency response using both Harmonic Balance and Secular Perturbation methods. We also look at the bistable solutions of the oscillator. A brief derivation of the Josephson relations, together with trial problems leading to Energy Participation Ratio (EPR) and qubits with positive anharmonicity, sets the stage for further understanding.

We then study some tools for superconducting circuit analysis, like circuit quantization, black-box quantization, EPR methods, and finite-element simulations. We then look at different qubit families, like the transmon qubit, a qubit with positive anharmonicity, flux qubit family and the unimon qubit.

As an exercise for these tools, we apply these tools to a transmon in a 3D cavity. We obtain and diagonalize the Lagrangian of the system, compute its EPRs from the resulting mode transformations, and analytically calculate the χ matrix. We also establish a bridge between EPR and black-box quantization. Numerical simulations performed in COMSOL further validate these results and we get a feel for practical values. Finally, we investigate systems composed of qubits with opposite anharmonicities and show analytically that their nonlinear interactions cancel to first order when their nonlinear coefficients match.

Contents

List of Figures

Chapter 1

Introduction

1.1 Introduction to Superconducting circuits

One of the platforms for implementing scalable quantum technology is superconducting circuits. These are macroscopic and can be printed in wafers, but also exhibit microscopic or quantum behavior. These can be customized to our needs; hence these are also called "Artificial atoms".

Analysis of these circuits makes use of the lumped circuit model. Here we assume that the properties of the circuit, like capacitance, inductance, and resistance, are idealized into electrical components, like capacitors, inductors, and resistors, joined together by perfectly conducting wires; hence the name "lumped".

In this architecture, we often need to induce anharmonicity, as the energy levels in a normal LC oscillator is linear, which is not desirable, as we wish to consider only the lowest states of the system in order to realize a qubit. This is done with the help of a Josephson junction, which introduces a cosine term in the Hamiltonian. As long as the Josephson energy is greater than the capacitive energy, the cosine potential can be expanded around $\phi = 0$ and the higher order can be treated perturbatively.

1.2 Motivation behind the project

Superconducting circuits are multi-mode systems by construction, where Josephson junctions interact with complex electromagnetic environments defined by cavities, transmission lines, and circuit modes. Traditional lumped-element models are often insufficient for capturing these interactions. Black-box quantization provides a powerful framework for deriving effective Hamiltonians directly from the simulated or measured impedance of a device, bypassing the need for oversimplified models. However, as systems become larger and more coupled, simply extracting mode spectra is not enough, and it also becomes computationally heavy.

Here, the Energy Participation Ratio (EPR) method is used. This quantifies how much each non-linear element participates in each normal mode, allowing an accurate calculation of anharmonicities, dispersive shifts, and coherence properties. Together, EPR and Black-box quantization provides a route to design and optimize superconducting quantum devices, bridging the gap between electromagnetic simulation and circuit Hamiltonians.

1.3 Summary and thesis outline

This thesis is about the various techniques to analyze superconducting qubits. Chapter 2 is about the theoretical background needed to understand the underlying physics of superconducting circuits, including a few trial problems. Chapter 3 describes the techniques used to analyze superconducting circuits. Chapter 4 studies the different types of qubits and a way to invoke positive anharmonicity into a circuit. Chapter 5 provides a detailed analysis of the transmon qubit in a 3D cavity, both analytically and numerically. Chapter 6 is about a theoretical construction of qubits with opposite anharmonicity and a toy problem to study the same.

Chapter 2

Theoretical background

In this chapter, we shall look at some prerequisites required to understand future concepts. Section 2.1 introduces Duffing oscillators, where we introduce non-linearity to a normal damped oscillator. This will be pivotal for understanding non-linearity in circuits. Section 2.2 will describe the Josephson effect and properties of Josephson junctions. They form a pivotal role in introducing non-linearity in superconducting devices. Section 2.3 will describe some trial problems done to understand the methodology of future chapters.

2.1 Duffing oscillator

Before we can analyze superconducting circuits, we need to understand the idea of nonlinearity and how it creeps into the system. This nonlinearity is essential for the anharmonicity of the qubit, which has many applications. To understand the same, we shall introduce the Duffing equation, which has a nonlinear term and it's analysis. We shall solve the Duffing equation using two methods, harmonic balance analysis and secular perturbation theory.

2.1.1 Introduction

We take the following one-dimensional differential equation

$$\ddot{x} + 2\gamma\dot{x} + \omega_0^2 x + \alpha x^3 = F_0 \cos(\omega t - \phi) \tag{2.1}$$

as evident, the equation without the αx^3 term is simply the equation of a forced dampened oscillator[3].

2.1.2 Harmonic balance analysis

We shall use the method of harmonic balance as mentioned in [4]. Looking for solutions of the form

$$x = a\cos(\omega t - \phi) \quad ,$$

using the necessary trigonometric substitutions, we obtain.

$$\begin{aligned}
&- a\omega^2(\cos\omega t\cos\phi + \sin\omega t\sin\phi) \\
&- 2\gamma a\omega(sin\omega t\cos\phi - \cos\omega t\sin\phi) \\
&+ \omega_0^2 a(\cos\omega t\cos\phi + \sin\omega t\sin\phi) \\
&+ \frac{3\epsilon a^3}{4}(\cos\omega t\cos\phi + \sin\omega t\sin\phi) \\
&\frac{\epsilon a^3}{4}(\cos 3\omega t\cos 3\phi + \sin 3\omega t\sin 3\phi) = F_0(\cos\omega t\cos\phi + \sin\omega t\sin\phi)
\end{aligned} \tag{2.2}$$

Finally, we discard the coefficients of the terms rotating three times the frequency, like $\cos 3\omega t$, equate the coefficients of $\cos\omega t$ and $\sin\omega t$ and eliminate ϕ by squaring both equations and adding them to get

$$a^2 = \frac{16F_0^2}{64\gamma^2\omega^2 + [\omega^2 - \frac{3}{4}\epsilon a^2 - \omega_0^2]^2} \tag{2.3}$$

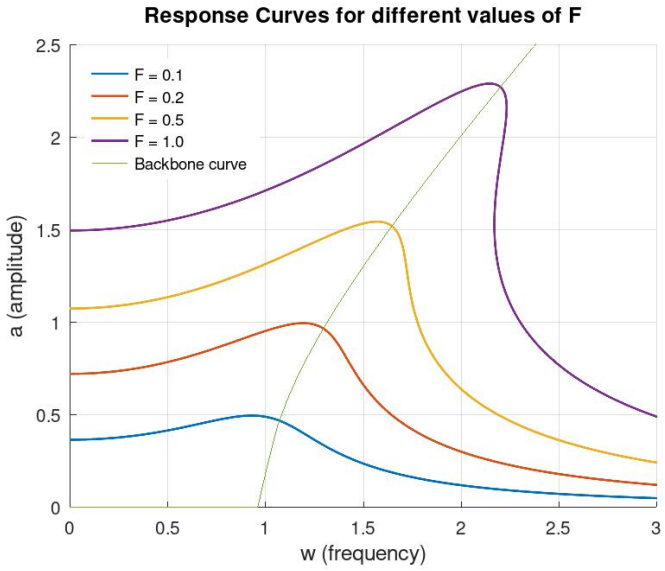

Figure 2.1: Plot of frequency vs amplitude for different driving forces. We have set $\omega_0 = 1, \gamma = 0.1, \epsilon = 1$

2.1.3 Secular perturbation theory

We also try the secular perturbation theory method as described in [5]. We first scale it for the ease of solving. We take $t' = \omega_0 t$ and $x' = x\sqrt{\alpha/m\omega_0^2}$. So dividing overall by $\omega_0^3\sqrt{m^3/\alpha}$
We obtain the equation

$$\ddot{x'} + Q^{-1}\dot{x'} + x' + x'^3 = G_0\cos(\omega' t' - \phi) \tag{2.4}$$

Where $\omega' = \omega/\omega_0$,$Q^{-1} = \frac{\gamma}{m\omega_0}$, $G_0 = \frac{F_0}{\omega_0^3}\sqrt{\frac{\alpha}{m^3}}$.
We now take the scaled equation 2.4. Now we take the limit of weak linear damping ϵ. This implies $Q^{-1} = \epsilon$ which is very less than unity. We also take $G_0 = \epsilon^{3/2}g$ as x is proportional to GQ, we want x to be of order $\sqrt{\epsilon}$ and Q is of order ϵ^{-1}
So 2.4 becomes

$$\ddot{x} + \epsilon\dot{x} + x + x^3 = \epsilon^{3/2}g\cos(1+\epsilon\Omega)t \tag{2.5}$$

Taking an amplitude of the order of $\sqrt{\epsilon}$, we assume a solution

$$x(t) = \frac{\sqrt{\epsilon}}{2}\left(A(T)e^{it} + \text{ Complex conj. }\right) + \epsilon^{3/2}x_1(t) + ... \tag{2.6}$$

where we take A(T) to be a quantity that slowly varies in time t, such that $T = \epsilon t$, and the lowest order contribution satisfies the linear harmonic oscillator solution. Rewrite A(T)

$$\dot{A} = \frac{dA}{dt} = \epsilon\frac{dA}{dT} = \epsilon A'$$

where we use the chain rule. Applying this ansatz

$$\dot{x} = \frac{\sqrt{\epsilon}}{2}([iA + \epsilon A']e^{it} + \text{Complex conj}) + \epsilon^{3/2}\dot{x}_1(t) + ... \tag{2.7}$$

$$\ddot{x} = \frac{\sqrt{\epsilon}}{2}([-A + 2i\epsilon A' + \epsilon^2 A'']e^{it} + \text{Complex conj}) + \epsilon^{3/2}\ddot{x}_1(t) + ... \tag{2.8}$$

Applying these in 2.16 and comparing the coefficients of $\epsilon^{3/2}$

$$\ddot{x}_1(t) + x_1(t) = \left[-iA' - \frac{i}{2}A + \frac{3}{8}|A|^2A + \frac{g}{2}e^{i\Omega t}\right]e^{it} - \frac{1}{8}A^3e^{3it} + c.c \tag{2.9}$$

The terms in the square brackets, which are the coefficients of e^{it} are the so called secular terms and they should vanish so that the solutions do not diverge (Note that this bears some similarity to the Harmonic Balance approach).

$$\implies A' = \frac{-1}{2}A + i\frac{3}{8}|A|^2A - i\frac{g}{2}e^{i\Omega t} \tag{2.10}$$

We ignore the initial transients and seek solution of the form

$$A(T) = ae^{i\Omega T} = |a|e^{i\phi}e^{i\Omega T} \tag{2.11}$$

So, the initial ansatz becomes

$$x(t) = \sqrt{\epsilon}|a|\cos(\omega t + \phi) + \mathcal{O}(\epsilon^{3/2}) \tag{2.12}$$

So now the amplitude-frequency relation becomes

$$i\Omega a e^{i\Omega T} = -\frac{1}{2}ae^{i\Omega T} + i\frac{3}{8}|a|^2 ae^{i\Omega T} - i\frac{g}{2}e^{i\Omega T} \tag{2.13}$$

Or simplifying, we get

$$g = \left[2\Omega - \frac{3}{4}|a|^2 + i\right]a \tag{2.14}$$

We can write this as

$$a^2 = \frac{g^2}{\left[\left(2\Omega - \frac{3}{4}|a|^2\right)^2 + 1\right]} \tag{2.15}$$

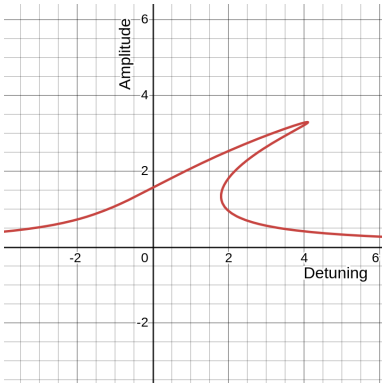

Figure 2.2: Plot of detuning vs amplitude, we have used Desmos for plotting.

We can reduce the regime of multi value solutions by adding a nonlinear damping term to 2.4, it becomes

$$\ddot{x} + \epsilon\dot{x} + x + x^3 + \eta\dot{x}x^2 = \epsilon^{3/2}g\cos(1 + \epsilon\Omega)t \tag{2.16}$$

Now the solution becomes

$$a^2 = \frac{g^2}{\left[\left(2\Omega - \frac{3}{4}|a|^2\right)^2 + (1 + \frac{\eta}{4}|a|^2)^2\right]} \tag{2.17}$$

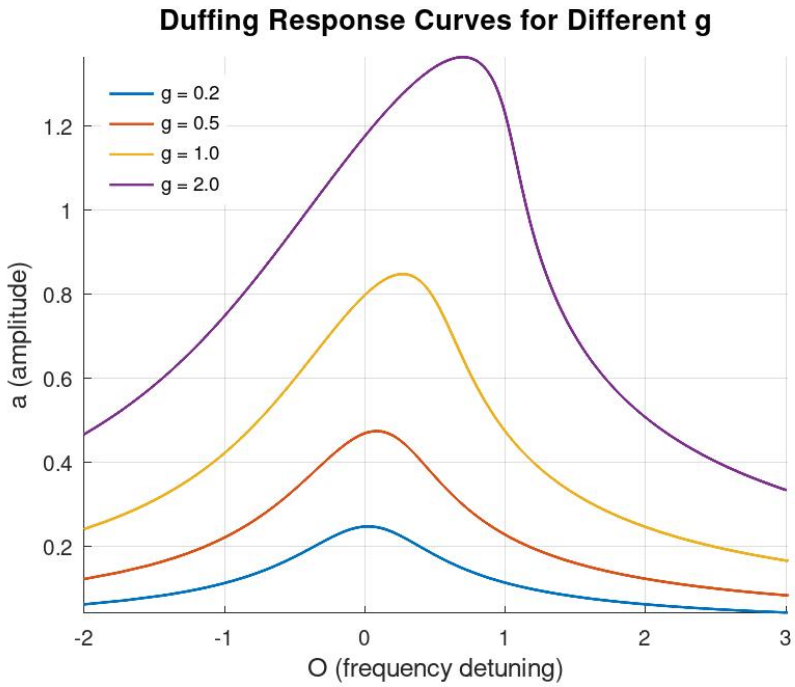

Figure 2.3: Plot of detuning vs amplitude for different g

2.1.4 Bistability of the Duffing oscillator

We take the equation obtained from Harmonic balance (2.3) and differentiate it with respect to a. We obtain

$$\frac{da}{d\omega} = \frac{8a\omega(-8\gamma^2 + 3a^2\epsilon + 4\omega_0^2 - 4\omega^2)}{27a^4\epsilon^2 + 48a^2\epsilon\omega_0^2 + 16\omega_0^4 + 64\gamma^2\omega^2 - 48a^2\epsilon\omega^2 - 32\omega_0^2\omega^2 + 16\omega^4} \tag{2.18}$$

By setting $da/d\omega = 0$, we get the frequency of the maximum amplitude or the backbone curve, which is

$$-8\gamma^2 + 3a^2\epsilon + 4\omega_0^2 - 4\omega^2 = 0 \tag{2.19}$$

This equation is sketched in Figure 2.1. Now we shall try finding the critical frequency where the onset of bifurcation occurs. We take the denominator and find the roots of ω and it turns out to be

$$\omega_{1\pm} = \pm\frac{1}{2}\sqrt{-8\gamma^2 + 6a^2\epsilon + 4\omega_0^2 - \sqrt{\Delta}} \tag{2.20}$$

$$\omega_{2\pm} = \pm\sqrt{-2\gamma^2 + \frac{3}{2}a^2\epsilon + \omega_0^2 + \frac{1}{4}\sqrt{\Delta}} \tag{2.21}$$

where

$$\Delta = 64\gamma^4 - 96a^2\gamma^2\epsilon + 9a^4\epsilon^2 - 64\gamma^2\omega_0^2$$

Discarding the negative values, we have two solutions. To get the critical frequency, setting $\Delta = 0$

$$\omega = \frac{1}{2}\sqrt{-8\gamma^2 + 6a^2\epsilon + 4\omega_0^2} \text{ for } a = \pm\frac{4\sqrt{2}\sqrt{-2\gamma^4 + 3\gamma^2\epsilon + 2\gamma^2\omega_0^2}}{3\epsilon} \tag{2.22}$$

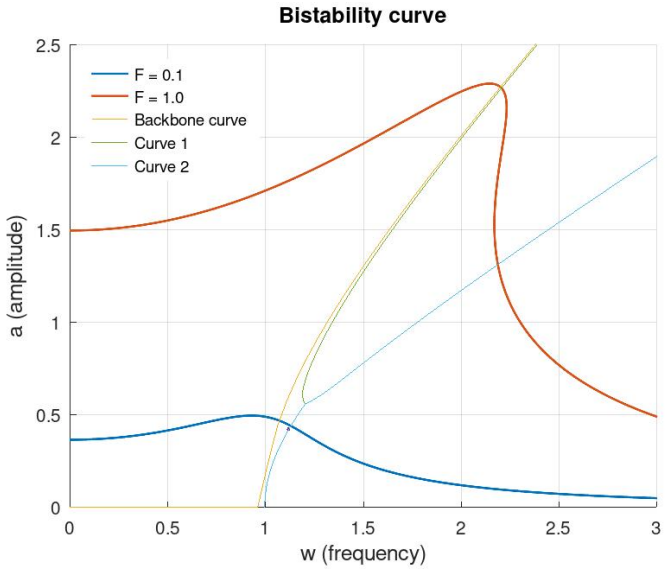

Figure 2.4: Plot of the bistable solutions of the Duffing oscillator

2.2 Josephson effect

In many cases, as we shall see, we may need to introduce a non-linearity in the circuits we design. One such device that helps in this regard is the Josephson junction [6], which consists of two superconducting electrodes separated by an insulator. We shall try to derive the energy of this system.

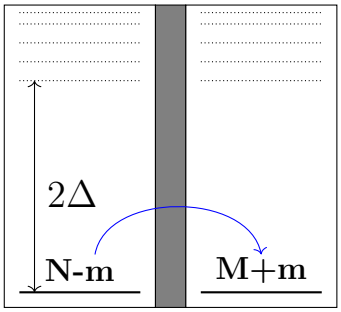

Figure 2.5: Image of a Josephson junction, containing two superconducting electrodes separated by an insulator. The image also shows tunneling between the electrodes. Note that 2Δ is the energy required to break the Cooper pair. Image inspired from [1]

.

We can roughly sketch the phenomenological Hamiltonian

$$H_T = -\frac{1}{2}E_J \sum_m \left[|m\rangle \langle m+1| + |m+1\rangle \langle m|\right], \tag{2.23}$$

where E_J is given by the Ambegaonkar-Baratoff relation

$$E_J = \frac{1}{2}\frac{h}{(2e)^2} G_N \Delta$$

Here, Δ is the energy required to break the pair of cooper pair, G_N is the conductance of the material. Seeking solutions of the form

$$|\varphi\rangle = \sum_{m=-\infty}^{\infty} e^{-im\varphi} |m\rangle, \tag{2.24}$$

we find that it satisfies the Schrodinger equation

$$H_T |\varphi\rangle = (-E_J \cos\varphi) |\varphi\rangle \tag{2.25}$$

To find the Josephson current, we obtain the group velocity

$$v_g(\varphi) = \frac{1}{\hbar}\frac{\partial}{\partial\varphi}(-E_J\cos\varphi) \tag{2.26}$$

and by multiplying 2e, we obtain Josephson's first relation.

$$I(\varphi) = 2ev_g(\varphi) = \frac{2e}{\hbar}(E_J\sin\varphi) = I_c\sin\varphi \tag{2.27}$$

2.3 Trial problems

2.3.1 Coupled mechanical oscillator

We take the simple system of a coupled mechanical oscillator as a toy problem to understand future concepts. The system is described by the diagram below

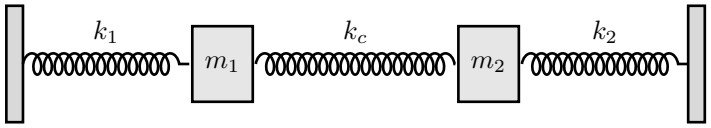

Figure 2.6: A schematic diagram of a coupled oscillator, coupled by the spring k_c

The Lagrangian can be written as

$$\mathcal{L} = \frac{1}{2}m_1\dot{q_1}^2 + \frac{1}{2}m_2\dot{q_2}^2 - \frac{1}{2}k_1q_1^2 - \frac{1}{2}k_2q_2^2 - \frac{1}{2}k_c(q_1-q_2)^2 \tag{2.28}$$

This can be written in matrix form as

$$\mathcal{L} = \frac{1}{2}\dot{\widetilde{Q}}^T M\dot{\widetilde{Q}} - \frac{1}{2}\widetilde{Q}^T K\widetilde{Q} \tag{2.29}$$

where

$$\widetilde{Q} = \begin{bmatrix}q_1\\q_2\end{bmatrix} \quad \dot{\widetilde{Q}} = \begin{bmatrix}\dot{q_1}\\\dot{q_2}\end{bmatrix} \quad M = \begin{bmatrix}m_1 & 0\\0 & m_2\end{bmatrix} \quad K = \begin{bmatrix}(k_1+k_c) & -k_c\\-k_c & (k_2+k_c)\end{bmatrix}$$

We can rewrite the Lagrangian as follows

$$\mathcal{L} = \frac{1}{2}\dot{Q}^T\dot{Q} - \frac{1}{2}Q^T\Omega^2 Q \tag{2.30}$$

where

$$Q = E\widetilde{Q} \tag{2.31a}$$

$$E = U^T M^{1/2} = \frac{1}{\sqrt{1+R_z^2}}\begin{pmatrix}\sqrt{m_1} & R_z\sqrt{m_2}\\-R_z\sqrt{m_1} & \sqrt{m_2}\end{pmatrix}, R_z = \frac{m_2(k_1+k_c) - m_1(k_2+k_c) + \sqrt{A^2+4m_1m_2B}}{2k_c\sqrt{m_1m_2}} \tag{2.31b}$$

$$U = \begin{bmatrix}cos\theta & -sin\theta\\sin\theta & cos\theta\end{bmatrix} = \frac{1}{\sqrt{1+R_z^2}}\begin{bmatrix}1 & -R_z\\R_z & 1\end{bmatrix}, \theta = \frac{1}{2}\tan^{-1}\left(\frac{\frac{2k_c}{\sqrt{m_1m_2}}}{\frac{k_1+k_c}{m_1} - \frac{k_2+k_c}{m_2}}\right) \tag{2.31c}$$

$$A = (k_1+k_c)m_2 + (k_2+k_c)m_1, B = k_1k_2 + k_c(k_1+k_2)$$

$$\Omega^2 = \begin{bmatrix}\omega_+^2 & 0\\0 & \omega_-^2\end{bmatrix} = E^T KE \tag{2.31d}$$

$$\omega_\pm = \frac{A \pm \sqrt{A^2+4m_1m_2B}}{2m_1m_2}; A = m_2(k_1+k_c) + m1(k_2+k_c); B = k_1k_2 + k_c(k_1+k_2) \tag{2.31e}$$

We define a new quantity called the participation ratio p_{mn} using matrix terms of U, u_{mn} where

$$p_{mn} = u_{mn}^2 \tag{2.32}$$

which gives the partipation ratio matrix

$$\Pi = \frac{1}{1+R_z^2}\begin{bmatrix} 1 & R_z^2 \\ R_z^2 & 1 \end{bmatrix} = \begin{bmatrix} p_{11} & p_{12} \\ p_{21} & p_{22} \end{bmatrix} \tag{2.33}$$

We can perform the Legendre transformation and obtain the Hamiltonian

$$H = \frac{1}{2}P^T P + \frac{1}{2}Q^T \Omega^2 Q \quad , \tag{2.34}$$

where P is the canonical momentum matrix obtained by

$$P = \begin{bmatrix} \mathbf{p}_1 \\ \mathbf{p}_2 \end{bmatrix} = \begin{bmatrix} \frac{\partial \mathcal{L}}{\partial \dot{q}_1} \\ \\ \frac{\partial \mathcal{L}}{\partial \dot{q}_2} \end{bmatrix}$$

2.3.2 Motivation and properties of the participation ratio matrix

We see that the elements of the participation ratio matrix describe how much each of the springs contributes to the energy of the mode. We shall analyze qubits with a similar quantity, called the Energy Participation Ratio (EPR), which describes how much each inductor contributes to the total energy of the system. We shall study more about this quantity in the next chapter.

Properties of Participation Matrix

Most of the properties of participation matrix arise because it is derived from a unitary transformation matrix.

- The elements of the Participation matrix are bounded as they are simply a ratio of inductive energy to total energy

$$0 \leq p_{mj} \leq 1 \tag{2.35}$$

- The total participation is conserved and add up to 1

$$0 \leq \sum_{m=1}^{M} p_{mj} \leq 1 \text{ for } j \in \{1, ..., J\} \tag{2.36}$$

- The total participation of a mode is at most unity

$$0 \leq \sum_{j=1}^{J} p_{mj} \leq 1 \tag{2.37}$$

- The columns of the unitary transformation matrix from which the participation matrix is derived, are orthogonal

$$\sum_{m=1}^{M} s_{mj} s_{mj'} \sqrt{p_{mj} p_{mj'}} = 0 \text{ for } j \neq j' \tag{2.38}$$

  meaning

$$u_{mj} = s_{mj} p_{mj}$$

  where s_{mj} is the sign of participation ratio.

2.3.3 Coupled quantum an-harmonic oscillator

We take the Hamiltonian.

$$\mathcal{H} = \frac{1}{2}k_1x_1^2 + \frac{p_1^2}{2m_1} + \alpha x_1^4 + \frac{1}{2}k_2x_2^2 + \frac{p_2^2}{2m_2} + \beta x_2^4 + gx_1x_2 \tag{2.39}$$

We group it into the form

$$\mathcal{H} = \mathcal{H}_0 + V$$

where

$$\mathcal{H}_0 = \frac{1}{2}k_1x_1^2 + \frac{p_1^2}{2m_1} + \frac{1}{2}k_2x_2^2 + \frac{p_2^2}{2m_2}$$

and the perturbation V is

$$V = \alpha x_1^4 + \beta x_2^4 + gx_1x_2$$

We can write the eigenvalues as

$$E_i = E_i^{(0)} + E_i^{(1)} + ...$$

Non-degenerate case

We know that the eigenvalues of the unperturbed system is

$$E_{n_1,n_2}^{(0)} = \hbar\omega_1(n_1 + \frac{1}{2}) + \hbar\omega_2(n_2 + \frac{1}{2}) \tag{2.40}$$

We apply the first-order perturbation and obtain

$$E_{n_1,n_2}^{(1)} = \alpha\frac{3\hbar^2}{4m_1^2\omega_1^2}(2n_1^2 + 2n_1 + 1) + \beta\frac{3\hbar^2}{4m_2^2\omega_2^2}(2n_2^2 + 2n_2 + 1) \tag{2.41}$$

We also perform the second order perturbation and obtain

$$E_{n_1,n_2}^{(2)} = \frac{g^2\hbar}{4m_1\omega_1m_2\omega_2}\frac{\omega_1(2n_2+1) - \omega_2(2n_1+1)}{w_2^2 - w_1^2} + \mathcal{O}(\alpha^2, \beta^2) \tag{2.42}$$

Combining all the above, we get the eigenvalue in the non-degenerate case as

$$\begin{aligned} E \approx \hbar\omega_1(n_1 + \frac{1}{2}) + \hbar\omega_2(n_2 + \frac{1}{2}) + \alpha\frac{3\hbar^2}{4m_1^2\omega_1^2}(2n_1^2 + 2n_1 + 1) + \beta\frac{3\hbar^2}{4m_2^2\omega_2^2}(2n_2^2 + 2n_2 + 1) \\ + \frac{g^2\hbar}{4m_1\omega_1m_2\omega_2}\frac{\omega_1(2n_2+1) - \omega_2(2n_1+1)}{w_2^2 - w_1^2} + ... \end{aligned} \tag{2.43}$$

Degenerate case

In the degenerate case, taking the states $|0\rangle$ and $|1\rangle$, we obtain the secular equation

$$\begin{vmatrix} \langle 00|\, V\, |00\rangle & \langle 01|\, V\, |01\rangle \\ \langle 10|\, V\, |10\rangle & \langle 11|\, V\, |11\rangle \end{vmatrix} = 0$$

We obtain the eigenvalue for the degenerate case as

$$E_{n_1,n_2} = \hbar\omega(n_1 + n_2 + 1) + (\alpha + \beta)\frac{9\hbar^2}{4m^2\omega^2} \pm \sqrt{(\alpha - \beta)^2\left(\frac{6h^2}{4m^2\omega^2}\right)^2 + \frac{g^2\hbar^2}{4\omega^2m^2}} \tag{2.44}$$

In the special case where $\alpha = -\beta$

$$E_{n_1,n_2} = \hbar\omega(n_1 + n_2 + 1) \pm \sqrt{(\alpha)^2\left(\frac{3h^2}{m^2\omega^2}\right)^2 + \frac{g^2\hbar^2}{4\omega^2m^2}} \tag{2.45}$$

2.4 Conclusion

This chapter provides a theoretical background for the analysis to be done in this thesis. We looked at how a nonlinear system behaves by taking the example of Duffing oscillator, and solved it using two methods. Then we looked at the Josephson effect and derived the Josephson relations using a phenomenological Hamiltonian. We finally looked at some trial problems from classical mechanics (coupled oscillators), quantum mechanics (coupled quantum anharmonic oscillators) and how it will manifest in our analysis of superconducting circuits

Chapter 3

Techniques used in analysis

In this chapter, we shall provide an overview of the different techniques used in the analysis of superconducting qubit designs. Section 3.1 describes the quantization techniques used in circuit QED such as the lumped element model to obtain the Hamiltonian of the circuit. It also describes how relevant these quantization techniques are for practical application. Section 3.2 describes the two main tools used for analysis in this thesis, the Blackbox quantization and the Energy Participation Ratio (EPR), how to obtain them and their applications. Section 3.3 briefly explains the finite element method used to numerically solve partial differential equations.

3.1 Circuit quantization and circuit QED

3.1.1 Introduction

Circuit QED is the study of interaction of non-linear circuits with quantized electromagnetic fields in the microwave domain. This has some ideas from cavity QED, which stems from principles of quantum optics and atomic physics, and has led to a deepened understanding of light matter interactions and quantum information.
The early era of the field of superconducting circuits started with the question of whether quantum phenomena can be observed in macroscopic systems, such as that of the Josephson junction [6]. The first evidence of such a question came with quantum tunneling of the phase degree of freedom of a Josephson junction, and the measurement of the quantized energy levels of the same [7].
Now that quantum phenomena can be observed in such systems, the possibility of coupling this with quantum computing has added more interest to this field. The combination of theoretical and experimental ideas from atomic physics and quantum optics and superconducting circuits led not only to exploration of this novel regime, but also to the realization of engineered quantum devices [8].

3.1.2 Circuit Quantization

We can treat circuit components smaller than the relevant wavelength as lumped elements [9]. In this section, we shall provide an example of an LC oscillator.
An LC oscillator has an inductor and capacitor in parallel, the Hamiltonian of the system is

$$H_{LC} = \frac{Q^2}{2C} + \frac{\Phi^2}{2L}, \tag{3.1}$$

where Q is the charge on the capacitor and Φ is the flux on the inductor. We can rewrite this in the familiar form of a linear oscillator

$$H_{LC} = \frac{Q^2}{2C} + \frac{1}{2}C\omega_r^2\Phi^2, \tag{3.2}$$

where $\omega_r = 1/\sqrt{LC}$. Now we can quantize the variables like in the case of a harmonic oscillator

$$[\hat{\Phi}, \hat{Q}] = i\hbar \tag{3.3}$$

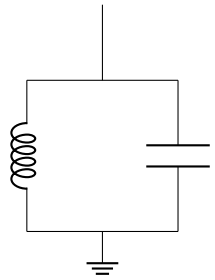

Figure 3.1: An LC circuit

We can also introduce creation and annihilation operators such as quantum harmonic oscillators

$$\hat{\Phi} = \Phi_{ZPF}(\hat{a}^\dagger + \hat{a}) \quad \hat{Q} = iQ_{ZPF}(\hat{a}^\dagger - \hat{a}) \tag{3.4}$$

where

$$\Phi_{ZPF} = \sqrt{\frac{\hbar}{2\omega_r C}} \quad Q_{ZPF} = \sqrt{\frac{\hbar\omega_r C}{2}}$$

we can rewrite the Hamiltonian as

$$\hat{H} = \hbar\omega_r(\hat{a}^\dagger\hat{a} + \frac{1}{2}) \tag{3.5}$$

3.1.3 Relevance of Quantization

One question that might arise is whether this quantization is relevant. The answer is that it is relevant if two conditions are satisfied

- The oscillator should be decoupled from uncontrolled degrees of freedom such that the energy levels are less broad than the separation ($Q = \omega_r/\kappa$, where Q is the Quality factor of the oscillator and κ is the linewidth).
- The energy separation between adjacent eigenstates ($\hbar\omega$) must be larger than the thermal energy ($k_B T$).

3.2 Techniques for Analysis of Qubits

3.2.1 Black box quantization (BBQ)

As qubit complexities increase, the coupling strength increases and the models derived from cavity QED struggle to incorporate this. So, the Black box quantization technique was introduced to address these issues [2]. The goal of BBQ is to find a basis that incorporates the main effect of coupling and perturbatively accounts for weak anharmonicity, assuming that charge dispersion is neglected.
Eg: Single Junction Case: If we take a system containing a Josephson junction having Josephson energy E_J and charging energy E_C in parallel with a linear electromagnetic environment, the Hamiltonian for the system is

$$H_{CPB} = 4E_C(\hat{N} - N_g)^2 - E_J cos(\hat{\varphi}) \tag{3.6}$$

Where $\hat{N}$ is the charge operator conjugate to $\hat{\varphi}$ and N_g is the offset charge. At low energies ($E_J >> E_C$), the quantum fluctuations of phase φ become small compared to π and the probability of tunneling becomes small. So we can expand the cosine term

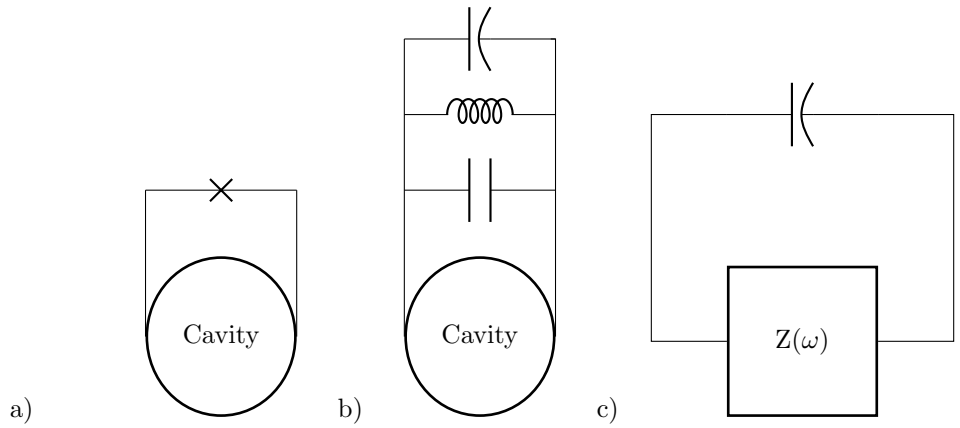

Figure 3.2: Schematic diagram of the process of Blackbox quantization. Here, a) is the Josephson junction coupled to the cavity. b) shows splitting of the Josephson junction into linear and nonlinear parts (denoted as a bent symbol). c) Shows the combination of the linear parts of Josephson junction and the cavity to form a "blackbox" while the ends of the non-linear part serves as the ports. Image inspired from [2]

An important quantity here is the impedance of the linear circuit $Z(\omega)$ which is a complicated function. But by virtue of Foster's theorem, this can be broken down to an equivalent circuit of parallel LCR oscillators

$$Z(\omega) = \sum_{p=1}^{M} \left(j\omega C_p + \frac{1}{j\omega L_p} + \frac{1}{R_p} \right)^{-1} \tag{3.7}$$

Where p is the mode, M is the total number of modes, C_p and L_p are the equivalent inductance and capacitance of each mode, and $j = -i$. This mapping corresponds to diagonalizing the linear harmonic oscillator circuits. The resonant frequencies will correspond to the poles of this inductance Z, or the roots of the admittance Y (where $Y(\omega) = Z^{-1}(\omega)$). For weak dissipation ($R_P >> \sqrt{L_p/C_p}$), this will come down to $1/\sqrt{L_p C_p}$. The imaginary part of the roots $(2R_pC_p)^{-1}$ gives the resonance a finite width and the effective capacitance can be found by the frequency derivative of admittance at the resonance point ($= \frac{1}{2} ImY'(\omega_p)$), which gives the expression for quality factor

$$Q_p = \frac{\omega_p}{2} \frac{ImY'(p)}{ReY(p)} \tag{3.8}$$

We can then find the decoherence time as follows

$$T_1 = \frac{Q_{qb}}{\omega_{qb}} \tag{3.9}$$

To find the low energy quantum Hamiltonian, we neglect dissipation, and construct the flux variable as

$$\phi_p = f_p e^{j\omega_p t} + f_p^* e^{-j\omega_p t} \tag{3.10}$$

for each LC oscillator. The Hamiltonian then becomes the following

$$\mathcal{H}_0 = 2 \sum_{p=1}^{M} (f_p)^* L_p^{-1} f_p \tag{3.11}$$

We can take the following variables

$$\phi_t = \sum_{p=1}^{M} \phi_p(t) \text{ where } \phi(t) = \int_{-\infty}^{t} V(\tau) d\tau \tag{3.12}$$

to an arbitrary constant. We also assume reduced flux

$$\varphi(t) = \frac{\phi(t)}{\phi_o} \mod 2\pi \qquad \phi_0 = \frac{h}{2e} \tag{3.13}$$

Introducing creation and annihilation operators

$$f_p^* = \sqrt{\frac{\hbar}{2} Z_p^{eff}} a_p^\dagger \qquad f_p = \sqrt{\frac{\hbar}{2} Z_p^{eff}} a_p \qquad Z_p^{eff} = \frac{2}{\omega_p Im Y'(\omega_p)} \tag{3.14}$$

we now rewrite the Hamiltonian as

$$\mathcal{H}_0 = \sum_p \hbar \omega_p a_p^\dagger a_p \tag{3.15}$$

and the flux operator across a junction can be written as

$$\hat{\phi} = \sum_{p=1}^{M} \sqrt{\frac{\hbar}{2} Z_p^{eff}} (a_p + a_p^\dagger) \tag{3.16}$$

Now we add the perturbation to the Hamiltonian

$$H = \mathcal{H}_0' + H_{nl} \text{ where } H_{nl} = \frac{-\phi^4}{24 \phi_0^2 L_J} + \mathcal{O}\left(\left(\frac{\hat{\phi}}{\phi_0}\right)^6\right) \tag{3.17}$$

Or, this can be rewritten as

$$H_4 = \mathcal{H}_0' + \frac{1}{2} \sum_{pp'} \chi_{pp'} \hat{n}_p \hat{n}_{p'} \tag{3.18}$$

where

$$\hat{n}_p = \hat{a}_p^\dagger a_p \; \mathcal{H}_0' = \mathcal{H}_0 + \sum_p \Delta_p \hat{n}_p \tag{3.19}$$

and Δ_p is the Lamb shift

$$\Delta_p = \frac{-e^2}{2L_J} \left(Z_p^{eff} \sum_q Z_q^{eff} - \frac{(Z_p^{eff})^2}{2} \right) \tag{3.20}$$

Now we see $\alpha_p = \chi_{pp}$ as the anharmonicity of the first excited state or the self-Kerr of mode p. We also see that $\chi_{pp'} = \chi_{p'p}$ is the state dependent frequency shift excitation or the anharmonicity of a mode p due to another mode p' (cross-Kerr). We can obtain the self Kerr and cross Kerr quantities from the impedances as

$$\chi_{pp} = -\frac{L_p}{L_J} \frac{C_J}{C_p} E_C \qquad \chi_{pp}' = -2\sqrt{\chi_{pp} \chi_{p'p'}} \tag{3.21}$$

3.2.2 Energy Participation Ratio (EPR)

The energy participation ratio, introduced by Minev et. al [10] is a useful tool for analyzing circuits. It provides a way to rewrite the Kerr terms in terms of quantities that are easier to find [8]. It also eliminates the need of finite element sweep, and instead relies on much simpler eigenmode analysis

Definition

The EPR describes how much of the inductive energy is stored in a Josephson junction. To give a rigorous definition, The EPR p_{mj} of the Josephson dipole j in eigenmode m is the fraction of inductive energy allocated to the Josephson dipole when the mode m is excited [10].

$$p_m = \frac{\text{Inductive energy present in the Josephson Junction}}{\text{Total inductive energy stored in the mode m}}$$

Analytical Method to obtain EPR

Analytically, EPR can be obtained from the unitary matrix used to diagonalize the Lagrangian [11]. the proof of this is shown here [11].

$$p_{mn} = \frac{\langle \Psi'_m | \frac{\phi_n^2}{2} | \Psi'_m \rangle}{\sum_l \langle \Psi'_m | \frac{\phi_l^2}{2} | \Psi'_m \rangle} \text{ (Energy stored in junction by the total energy of the mode)} \tag{3.22}$$

$$= \frac{\langle \Psi'_m | (\sum_k u_{kn} \phi'^2_k)^2 | \Psi'_m \rangle}{\sum_l \langle \Psi'_m | \frac{\phi_l^2}{2} | \Psi'_m \rangle} \text{ (Unitary transformation of the variable)} \tag{3.23}$$

$$= u_{mn}^2 \frac{\langle \Psi'_m | \Phi_m | \Psi'_m \rangle}{\langle \Psi'_m | \Phi_m | \Psi'_m \rangle} \text{ (Orthogonality)} \tag{3.24}$$

$$p_{mn} = u_{mn}^2 \tag{3.25}$$

Numerical calculation of EPR for single Josephson junction

In the case of single Josephson junction, we can directly use the global electrical and magnetic eigenmode energies to obtain the EPR of the mode p_m [10].

$$p_m = \frac{\mathcal{E}_{electrical} - \mathcal{E}_{magnetic}}{\mathcal{E}_{electrical}} \tag{3.26}$$

Numerical calculation of EPR for multiple Josephson junctions

For the case of multiple junctions, the EPR takes the following form [10].

$$p_{mj} = \frac{\frac{1}{2} L_j I_{m,j}^2}{\mathcal{E}_{ind}} \tag{3.27}$$

The current I_{mj} can be calculated by

$$|I_{mj}| = l_j^{-1} \int_{S_i} |\vec{J}_{s,m}| ds \tag{3.28}$$

where l_j is the length of the sheet.

Analogy to the trial problem

As is evident, the EPR obtained from the analytical method matches the participation ratio introduced in Section 2.3. As we have looked at the properties of participation ratio already, it will now be easy to summarize the properties of EPR obtained here as well, which we shall do now.

Properties of EPR

- **EPR is bounded**

$$0 \leq p_{mj} \leq 1 \tag{3.29}$$

- **The total EPR is conserved**

$$0 \leq \sum_{m=1}^{M} p_{mj} \leq 1 \text{ for } j \in \{1, ..., J\} \tag{3.30}$$

- **The total EPR of a mode is at most unity**

$$0 \leq \sum_{j=1}^{J} p_{mj} \leq 1 \tag{3.31}$$

- **The vector EPRs of two dipoles are orthogonal**

$$\sum_{m=1}^{M} s_{mj} s_{mj'} \sqrt{p_{mj} p_{mj'}} = 0 \text{ for } j \neq j' \tag{3.32}$$

Applications of EPR

1. Writing the nonlinear terms in terms of EPR

$$\varphi_j^2 = p_j \frac{\hbar\omega_j^2}{2E_J} \tag{3.33}$$

2. Writing the Kerr matrix in terms of EPR

$$\chi = \frac{\hbar}{4}\Omega\Pi E_J^{-1}\Pi^T\Omega \tag{3.34}$$

$$\alpha_m = \frac{1}{2}\chi_{mm} \tag{3.35}$$

$$\Delta_m = \sum_{m'=1}^{M} \chi_{mm'} \tag{3.36}$$

3.3 Finite Element Method and COMSOL

Most of the laws in physics are expressed in terms of partial differential equations (PDEs). For most problems having complex geometries, the obtained PDEs cannot be solved analytically. Instead, an approximation of equations can be constructed, based on different types of discretizations, which approximate these PDEs into numerical model equations. The solutions of these equations are approximate real solutions of PDEs [12].
Seeking solutions of the form

$$u(x,y) = \sum_{i=1}^{n} a_i\phi_i(x,y) = u(x,y,a) \tag{3.37}$$

Where ϕ_i are basis functions and a_i can be found by substituting the solution into the differential equation and minimizing the residue [13].
These are special forms of expansion methods where basis functions are finite elements, meaning that there are negligible everywhere except for the small part of the domain. The steps involved are

1. Partition the region where solution is required into convenient pieces.
2. Over each piece, define a basis function that is zero everywhere else except for that piece. The piecewise approximation should satisfy continuity, as in it should be continuous across the boundaries of two pieces. In order to ensure continuity, we can define basis functions in terms of function points at suitably chosen nodes or nodal points.
3. Substitute this basis function into the differential equation and obtain an algebraic equation.
4. Solve the algebraic equation to obtain the coefficients of expansion.

3.4 Conclusion

In this chapter, we have presented some tools for studying superconducting quantum circuits, starting with the lumped circuit model and circuit quantization. Then we follow it up with Black box quantization where we treat the linear elements as a black box and find resonance frequencies through a frequency sweep. We also saw how to obtain useful quantities from the same. Then we studied the concept of energy participation ratio, methods of obtaining it both analytically and numerically, and it's application in finding out self and cross Kerr values and anharmonicities. We finally conclude the chapter by learning about the finite element method, which will be useful when doing simulations.

Chapter 4

Study of different types of qubits

In this chapter, we shall introduce a few popular qubits and their Hamiltonians that are used for analysis. Section 4.1 describes in brief, the transmon qubit and it's Hamiltonian. Section 4.2 is about how to design a qubit that has positive anharmonicity. Section 4.3 is about the flux qubit and its family, describing the various designs that have the same basic property. Section 4.4 introduces the Fluxonium qubit and the derivation of it's Hamiltonian. Section 4.5 introduces the Unimon qubit, it's design and its Hamiltonian.

4.1 Transmon qubit

The transmon qubit was introduced by Koch et al. [14] as a modification to the primitive Cooper pair box qubit. It is currently the most popular qubit variety. It's basic design consists of a large shunt capacitance parallel to the Josephson junction, thus reducing E_C and thus reducing charge dispersion.

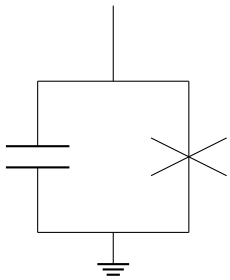

Figure 4.1: Equivalent circuit diagram of a Transmon qubit

The Hamiltonian of this qubit can be written as

$$H = \frac{Q^2}{2C} - E_J cos\phi \tag{4.1}$$

Analysis of the transmon qubit, both analytically and numerically, is done extensively in Chapter 5.

4.2 Qubit with positive anharmonicity

We shall now look at how to obtain qubits with positive anharmonicity. The motivation behind this is that it can be used to model two level atoms and selectively raise even levels. We can also lower ZZ interactions if we have two qubits with opposite anharmonicities [15] [16]. We take the circuit as shown below

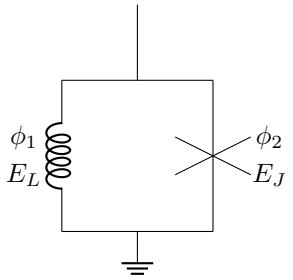

Figure 4.2: Equivalent circuit diagram of a qubit with positive anharmonicity

Taking the potential energy

$$U = \frac{E_L \phi_1^2}{2} - E_J cos(\phi_2) \tag{4.2}$$

Using the flux quantization condition

$$\phi_1 - \phi_2 = 2\pi \frac{\Phi_{ext}}{\phi_0}$$

Setting $\frac{\Phi_{ext}}{\phi_0} = \frac{1}{2}$, and substituting in 4.2

$$U = \frac{E_L \phi_1^2}{2} - E_J cos(\pi + \phi_1) = \frac{E_L \phi_1^2}{2} + E_J cos(\phi_1) \tag{4.3}$$

The cosine term has become positive, implying the first anharmonic term ($\mathcal{O}(\phi^4)$) has a positive sign. So this qubit is a positively anharmonic qubit at the sweet spot $\frac{\Phi_{ext}}{\phi_0} = \frac{1}{2}$.

4.3 Flux qubit

The flux qubit was first introduced by Friedman et.al [17], based on the principle that a superconducting loop interrupted by a Josephson junction, can exist in a superposition of clockwise and anticlockwise current flow states (which are distinguishable macroscopic quantities)[18]. There exists a family of qubits following the property, which are listed below

4.3.1 Three-junction flux qubit

The three-junction flux qubit is the most common choice in this family. It consists of three Josephson junctions, out of which two are similar and larger (say by a factor of γ) than the third one in the middle. We can write the potential energy of this system as

$$\begin{aligned} U &= -\gamma E_J \cos(\phi_1) - \gamma E_J \cos(\phi_2) - E_J \cos(\phi_3) \\ &= -2\gamma E_J \cos\left(\frac{\phi_1 - \phi_2}{2}\right) \cos\left(\frac{\phi_1 + \phi_2}{2}\right) - E_J cos(\phi_3) \end{aligned} \tag{4.4}$$

Using the flux quantization condition

$$\phi_1 + \phi_2 + \phi_3 = 2k\pi \implies \phi_3 = 2k\pi - \phi_1 + \phi_2$$

where $k = \phi_{ext}/\phi_0$ the equation becomes,

$$U = -2\gamma E_J \cos\left(\frac{\phi_1 - \phi_2}{2}\right) \cos\left(\frac{\phi_1 + \phi_2}{2}\right) - E_J \cos(2k\pi - (\phi_1 + \phi_2)) \tag{4.5}$$

4.3.2 C-Shunted flux qubit

The E_c can be reduced by introducing a large shunt capacitance in parallel to the Josephson junctions [18] [19]. This leads to improvement in coherence time and decay time while preserving anharmonicity.

4.4 Fluxonium qubit

The fluxonium qubit consists of a Josephson junction shunted by a large array of Josephson junctions. The potential energy is given by

$$U = -E_J cos\Phi - \sum_{i=1}^{N} E_i cos\phi_i \tag{4.6}$$

where i is the index of the Josephson junction. Taking the Josephson junction in the array to be identical having the Josephson energy E and applying the flux condition.

$$N\phi = \Phi \implies \sum_{i=1}^{N} E_i cos\phi_i = NE\cos\frac{\Phi}{N}$$

Putting this back in 4.6 we get

$$U = -E_J cos\Phi - NE\cos\frac{\Phi}{N}$$

Taking N to a very large number and neglecting the constant term, we obtain the potential energy of the fluxonium as

$$U = -E_J cos\Phi + NE\frac{\Phi^2}{2N^2} = -E_J cos\Phi + E_L\frac{\Phi^2}{2} \tag{4.7}$$

where $E_L = \frac{E}{N}$

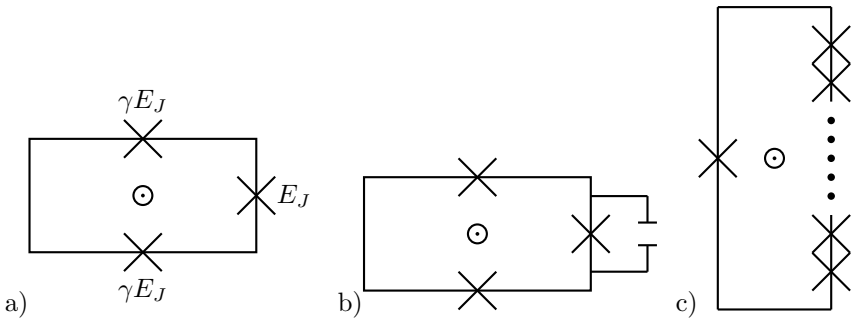

Figure 4.3: Qubit designs belonging to the Flux qubit family. Here, a) is the typical three-junction flux qubit, b) is the the C-shunted flux qubit and c) is the fluxonium qubit

4.5 Unimon qubit

Unimon qubit was introduced by Hyyppa et. al [20], as an alternative to transmon and flux qubit family. The design consists of a Josephson junction connected with coplanar waveguides (CPWs) on both sides.

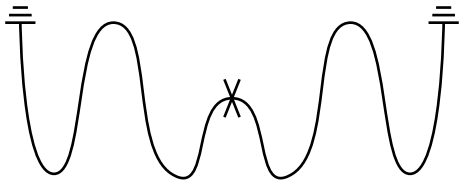

Figure 4.4: Schematic diagram of the Unimon qubit

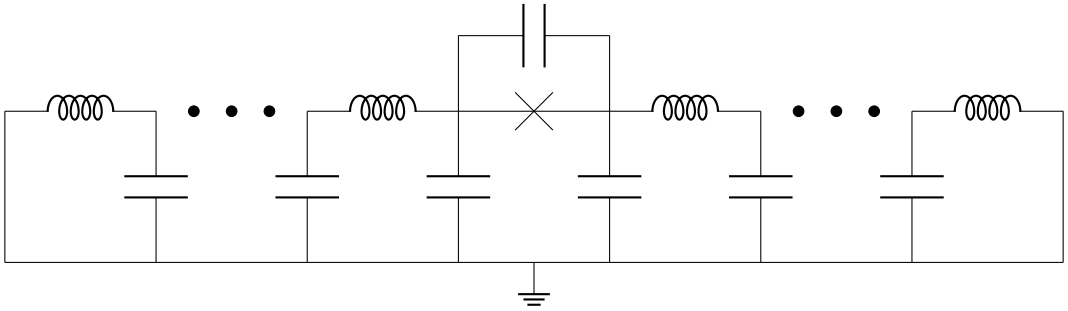

Figure 4.5: Circuit diagram of the Unimon qubit

The Hamiltonian for a qubit mode m is given by [20]

$$\hat{H}_m = 4E_{C,m}(\varphi_0)\hat{n}_m^2 + \frac{1}{2}E_{L,m}(\varphi_0)\hat{\varphi}_m^2 + E_L\hat{\varphi}_m\left(\frac{2\pi\Phi_{diff}}{\Phi_0} - \varphi_0\right) - E_J\cos(\hat{\varphi}_m - \varphi_0) \quad , \tag{4.8}$$

where $E_{C,m}$ is the capacitive energy of the qubit mode, E_L is the inductor energy, E_J is the Josephson energy, $E_{L,m}$ is the inductive energy.
At the sweet spot $\Phi_{diff}/\Phi_0 = \frac{1}{2}, \varphi_0 = \pi$ and the Hamiltonian reduces to

$$\hat{H}_m = 4E_{C,m}(\pi)\hat{n}_m^2 + \frac{1}{2}E_{L,m}(\pi)\hat{\varphi}_m^2 + E_J\cos(\hat{\varphi}_m) \quad , \tag{4.9}$$

where we assume $E_J \leq E_L$. Taylor expanding the cosine term

$$\hat{H}_m = 4E_{C,m}(\pi)\hat{n}_m^2 + \frac{1}{2}(E_{L,m}(\pi) - E_J)\hat{\varphi}_m^2 + \frac{E_J}{24}\hat{\varphi}_m^4 + \mathcal{O}(\hat{\phi}^6 k) \tag{4.10}$$

4.6 Conclusion

In this section, we have looked at different types of superconducting qubits. We introduced briefly the transmon qubit, on which we shall do a detailed analysis in the next chapter. Then we introduced a way to invoke positive anharmonicity in a qubit, and then explored qubit options to implement the same, like the flux qubit family, the fluxonium qubit and the unimon qubit. This chapter serves as an introduction to the general types of qubit designs in the superconducting qubit architecture.

Chapter 5

Analytical and Numerical computation for a Transmon qubit in a 3D cavity

5.1 Introduction

This section discusses the calculations for the transmon qubit, coupled to a three dimensional rectangular cavity, both analytically and numerically. Section 5.2 describes in detail, the Lagrangian of the circuit, diagonalizing it using the methods discussed earlier. The section also discusses, in brief, a method to obtain the eigenfrequencies of the transmon coupled to a 3-D cavity, and in brief about the quantization of Hamiltonian and the concept of avoided crossing. Section 5.3 is about analytically obtaining the EPR in terms of inductances and capacitances of the circuit. We also calculate the χ matrix using the EPR result obtained. Section 5.4 derives the χ matrix relation of blackbox by tweaking the χ matrix and EPR relation. It also describes how to obtain the admittance function, which the blackbox method requires, using EPR and eigenfrequencies. Section 5.5 explains how the system is set up in COMSOL, for the finite element method, the data obtained from such a simulation and analysis of the data to obtain the values of χ matrix, quality factor and decoherence time.
We construct a 3D cavity in the following way

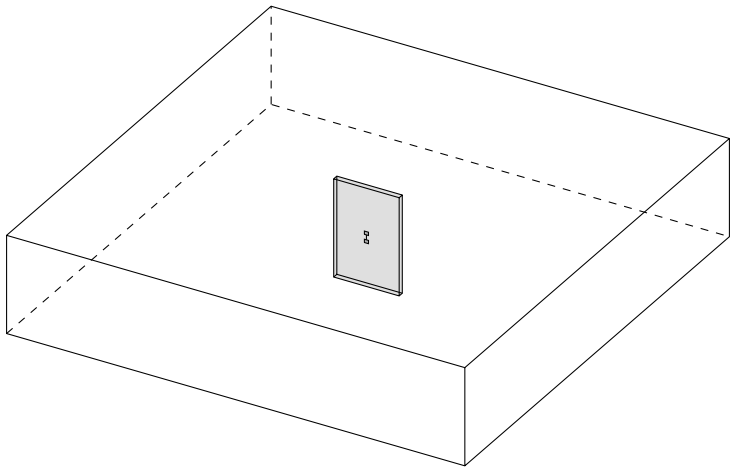

Figure 5.1: Construction of a transmon qubit along with the measuring cavity

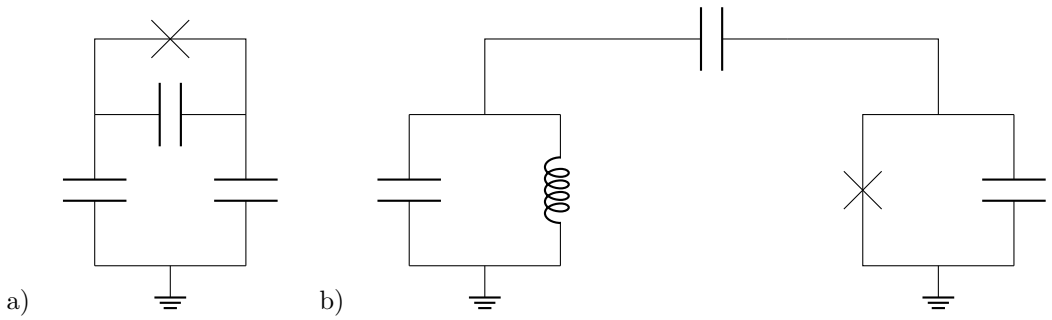

Figure 5.2: a) Lumped circuit of the Transmon design b) Lumped circuit of the Transmon in 3D cavity

5.2 Obtaining the Hamiltonian of the circuit

The Lagrangian for this circuit can be written as

$$\mathcal{L} = \frac{1}{2}C_r\dot{\varphi_1}^2 + \frac{1}{2}C_q\dot{\varphi_2}^2 + \frac{1}{2}C_c(\dot{\varphi_1} - \dot{\varphi_2})^2 - \frac{\varphi_1^2}{2L_r} - E_J cos(\varphi_2) \tag{5.1}$$

Or, this can be simplified as

$$\mathcal{L} = \frac{1}{2}(C_r + C_c)\dot{\varphi_1}^2 + \frac{1}{2}(C_q + C_c)\dot{\varphi_2}^2 - C_c\dot{\varphi_1}\dot{\varphi_2} - E_J cos(\varphi_2) - \frac{\varphi_1^2}{2L_r} \tag{5.2}$$

5.2.1 Diagonalizing the Lagrangian

Taylor expanding the cosine term and ignoring the constant offset,

$$\mathcal{L} = \frac{1}{2}(C_r + C_c)\dot{\varphi_1}^2 + \frac{1}{2}(C_q + C_c)\dot{\varphi_2}^2 - C_c\dot{\varphi_1}\dot{\varphi_2} - \frac{\varphi_1^2}{2L_r} - \frac{1}{2}E_J(\varphi_2)^2 + \mathcal{L}_{nl} \tag{5.3}$$

where

$$\mathcal{L}_{nl} = -E_J cos(\varphi_2) + \frac{1}{2}E_J(\varphi_2)^2$$

We can write this in the matrix form as

$$\mathcal{L} = \frac{1}{2}\dot{\Phi}^T\mathbf{C}\dot{\Phi} - \frac{1}{2}\Phi^T\mathbf{L}^{-1}\Phi + \mathcal{L}_{nl} \tag{5.4}$$

where

$$\mathbf{C} = \begin{bmatrix} C_r + C_c & -C_c \\ -C_c & C_q + C_c \end{bmatrix} \tag{5.5}$$

$$\mathbf{L}^{-1} = \begin{bmatrix} \frac{1}{L_r} & 0 \\ 0 & \frac{1}{L_J} \end{bmatrix} \quad , \tag{5.6}$$

where $L_J = \frac{1}{E_J}$ and note that we are working on a reduced flux basis. We first scale Φ so that

$$\Phi_s = L^{-1/2}\Phi \tag{5.7}$$

so now the equation becomes

$$\mathcal{L} = \frac{1}{2}\dot{\Phi}_s^T\mathbf{C}_s\dot{\Phi}_s - \frac{1}{2}\Phi_s^T\mathbf{I}_L\Phi_s + \mathcal{L}_{nl(s)} \tag{5.8}$$

Where $L_{nl(s)}$ is the nonlinear element scaled, and

$$C_s = L^{1/2}CL^{1/2} = \begin{bmatrix} L_r(C_r + C_c) & -C_c\sqrt{L_rL_J} \\ -C_c\sqrt{L_rL_J} & L_J(C_q + C_c) \end{bmatrix} \tag{5.9}$$

Diagonalizing C_s, we obtain

$$R^TC_sR = \Lambda = \begin{bmatrix} D_+ & 0 \\ 0 & D_- \end{bmatrix} \text{ where } R = \begin{bmatrix} \cos\theta & -\sin\theta \\ \sin\theta & \cos\theta \end{bmatrix} \tag{5.10}$$

$$\tan 2\theta = \frac{2C_c\sqrt{L_rL_J}}{L_r(C_r+C_c)-L_J(C_q+C_c)}$$

We obtain

$$D_\pm = \frac{L_r(C_r+C_c)+L_J(C_q+C_c)}{2} \pm \frac{1}{2}\sqrt{(L_r(C_r+C_c)-L_J(C_q+C_c))^2+4C_c^2L_rL_J} \tag{5.11}$$

Now looking at the rotation matrix, we can write it in terms of the inductances and capacitances as

$$R = \begin{bmatrix} \sqrt{\frac{D+A}{2D}} & -\frac{B}{\sqrt{2D(D+A)}} \\ \frac{B}{\sqrt{2D(D+A)}} & \sqrt{\frac{D+A}{2D}} \end{bmatrix} \tag{5.12}$$

where

$$A = L_r(C_r+C_c)-L_J(C_q+C_c) \qquad B = -2C_c\sqrt{L_rL_J}$$
$$D = \sqrt{(L_r(C_r+C_c)-L_J(C_q+C_c))^2+4C_c^2L_rL_J}$$

Now rewriting the Lagrangian

$$\mathcal{L} = \frac{1}{2}(\dot{\Phi}_s^T R)R^T\mathbf{C}_sR(R^T\dot{\Phi}_s) - \frac{1}{2}\Phi_s^T\mathbf{I}_L\Phi_s + \mathcal{L}_{nl(s)}$$

$$\mathcal{L} = \frac{1}{2}\dot{\Phi}_m^T\Lambda\dot{\Phi}_m - \frac{1}{2}\Phi_m^T\mathbf{I}_L\Phi_m + \mathcal{L}_{nl}(\Phi_m) \tag{5.13}$$

where we do the following transformations

$$\Phi_m = R^T\Phi_s \text{ and } \mathcal{L}_{nl}(\Phi_m) = \mathcal{L}_{nl}(\Phi_t(\Phi_m))$$

Hence we have successfully diagonalized the Lagrangian, and we are set to obtain the Hamiltonian of the circuit.

5.2.2 Obtaining the Hamiltonian of the Circuit

We find the equation of motion for the Lagrangian by using the Euler Lagrange equation

$$\frac{d}{dt}\frac{\partial\mathcal{L}}{\partial\dot{\Phi}_m} - \frac{\partial\mathcal{L}}{\partial\Phi_m} = 0$$

We obtain

$$\frac{d^2}{dt^2}\Phi_m + \Omega^2\Phi_m = 0 \tag{5.14}$$

Where $\Omega^2 = \Lambda^{-1}$ having the dimensions of ω^2 Now the canonical momentum is given by

$$Q_m = \frac{\partial\mathcal{L}}{\partial\dot{\Phi}_m} = \Lambda\dot{\Phi}_m \tag{5.15}$$

Performing the Legendre transformation, we obtain the Hamiltonian of the circuit as

$$H = (\dot{\Phi}_m)^TQ_m - \mathcal{L}$$
$$H = Q_m^T\Omega^2Q_m + \Phi_m^TI_L\Phi_m + H_{nl} \tag{5.16}$$
$$H_{nl} = -\mathcal{L}_{nl}$$

Now we have

$$\Omega = \begin{bmatrix} \omega_+ & 0 \\ 0 & \omega_- \end{bmatrix} \tag{5.17}$$

We get the frequencies in terms of the inductances and capacitances as

$$\omega_\pm = \left(\frac{L_r(C_r+C_c)+L_J(C_q+C_c)}{2} \pm \frac{1}{2}\sqrt{(L_r(C_r+C_c)-L_J(C_q+C_c))^2+4C_c^2L_rL_J}\right)^{-1/2} \tag{5.18}$$

5.2.3 Quantizing the Hamiltonian

We introduce the action angle variables

$$\alpha(t) = \frac{1}{2\hbar\Omega}\left(\Phi_m(t) + i\Omega Q_m(t)\right) \tag{5.19}$$

such that the Poisson bracket becomes

$$\{\alpha_m, \alpha_n^*\} = \frac{1}{i\hbar}\delta_{mn}$$

Using this, we rewrite the Hamiltonian as follows.

$$H = \frac{\hbar}{2}\left(\alpha^T\Omega\alpha^* + \alpha^{*T}\Omega\alpha\right) + H_{nl}(\alpha, \alpha^*) \tag{5.20}$$

Using Dirac's method to quantize the action angle variables to creation and annihilation operators, the Poisson bracket simply becomes a commutator

$$\alpha_m \to \hat{a}_m, \alpha_m^* \to \hat{a}_m^\dagger, i\hbar\{\alpha_m, \alpha_n^*\} \to [\hat{a}_m, \hat{a}_n^\dagger] = \delta_{mn}$$

Now the Hamiltonian takes the familiar form

$$\hat{H} = \sum_{m=1}^{M} \hbar\omega_m \hat{a}_m^\dagger \hat{a}_m + \hat{H}_{nl} \tag{5.21}$$

where

$$\hat{H}_{nl} = \sum_{p=3}^{\infty} E_J c_p \hat{\varphi}^p$$

Where φ can be written in terms of creation and annihilation operators as

$$\hat{\varphi}_m = \sqrt{\frac{\hbar\omega_m}{2}}(a_m + a_m^\dagger)$$

We can extend this to the matrix to find the zero point fluctuation

$$\hat{\Phi}_m = \Phi_m^{ZPF}(\hat{a} + \hat{a}^\dagger) \tag{5.22a}$$
$$\hat{Q}_m = iQ_m^{ZPF}(\hat{a} - \hat{a}^\dagger) \tag{5.22b}$$

where

$$\Phi_m^{ZPF} = \sqrt{\frac{\hbar}{2}}\Omega_{1/2} \tag{5.22c}$$
$$Q_m^{ZPF} = \sqrt{\frac{\hbar}{2}}\Omega^{-1/2} \tag{5.22d}$$

5.2.4 Avoided crossing of the eigenfrequencies

We can approximately rewrite the eigenfrequency expression as

$$\omega_\pm \approx \frac{1}{2}(\omega_1 + \omega_2) \pm \frac{1}{2}\sqrt{(\omega_1 - \omega_2)^2 + 4g^2} \tag{5.23}$$

where

$$\omega_1 = \frac{1}{\sqrt{L_r(C_r + C_c)}} \quad \omega_2 = \frac{1}{\sqrt{L_J(C_q + C_c)}} \quad g = \frac{C_c}{2\sqrt{(C_r + C_c)(C_q + C_c)}}\sqrt{\omega_1\omega_2}$$

If we vary L_J so that $\omega_1 = \omega_2$, then we see the avoided crossing, the shortest distance between the two curves will provide the value of 2g, which is a measure of the coupling of the modes.

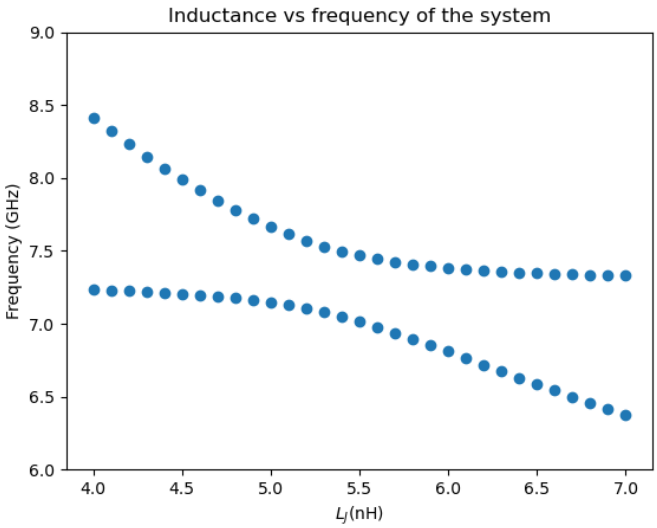

Figure 5.3: Demonstration of avoided crossing

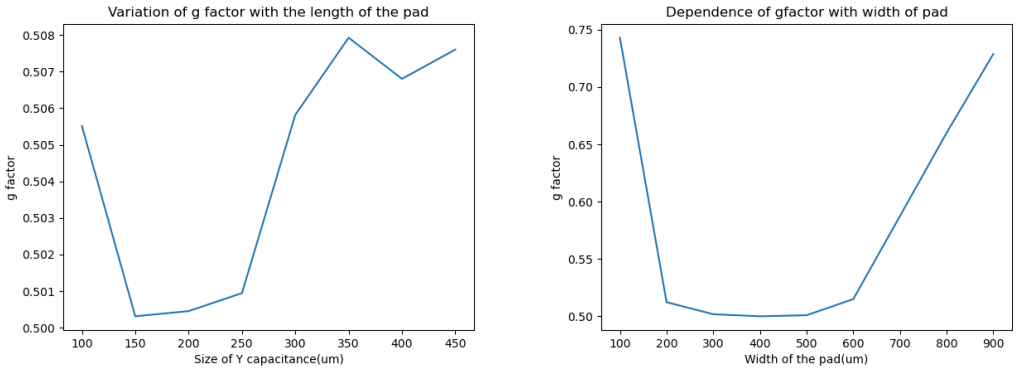

Figure 5.4: Variation of g factor with the length and width of the pad, as simulated in COMSOL

5.3 Analytical EPR analysis

We shall now do the analytical calculation of EPR. From 3.2.2, we see that we can obtain EPR from the rotation matrix, which in this case is 5.12. Squaring the elements, we obtain the EPR matrix as

$$\Pi = \begin{bmatrix} \frac{D+A}{2D} & \frac{B^2}{2D(D+A)} \\ \frac{B^2}{2D(D+A)} & \frac{D+A}{2D} \end{bmatrix} = \begin{bmatrix} p_1 & p_2 \\ p_2 & p_1 \end{bmatrix} \tag{5.24}$$

where

$$A = L_r(C_r + C_c) - L_J(C_q + C_c) \qquad B = 2C_c\sqrt{L_r L_J}$$
$$D = \sqrt{(L_r(C_r + C_c) - L_J(C_q + C_c))^2 + 4C_c^2 L_r L_J}$$

From 5.24 we can see, Π satisfies all the properties of EPR. Now we calculate χ matrix as

$$\chi = (\Omega\Pi)E_J^{-1}\Pi^T\Omega \tag{5.25}$$

In this case,

$$E_J^{-1} = \begin{bmatrix} \frac{1}{E_J} & 0 \\ 0 & 0 \end{bmatrix}$$

which gives the χ matrix as

$$\chi = \begin{bmatrix} \frac{\hbar\omega_+^2}{4E_J}p_1^2 & \frac{\hbar\omega_+\omega_-}{4E_J}p_1p_2 \\ \frac{\hbar\omega_+\omega_-}{4E_J}p_1p_2 & \frac{\hbar\omega_-^2}{4E_J}p_2^2 \end{bmatrix} \tag{5.26}$$

Now we have the self and cross Kerr terms with respect to the inductances and capacitances of the circuit.

5.4 Analytical Blackbox analysis

We take the equation obtained in Blackbox quantization

$$\chi_{pp} = -\frac{L_p}{L_J}\frac{C_J}{C_p}E_C$$

By multiplying L_J on both the numerator and the denominator, converting this form into an energy form by dividing $\hbar$ and using $C_J = e^2/2E_C$, $C_p = 1/\omega_p^2 L_p$ and $E_J = \Phi_0^2/L_J$ and manipulating, we obtain the following

$$\chi_{pp} = -\frac{L_p^2}{L_J^2}\frac{\hbar\omega_p^2}{4E_J} \tag{5.27}$$

Now taking $L_p^2/L_J^2 = p_p^2$ we obtain the χ matrix relation obtained from our EPR analysis. We can obtain equivalent inductance of a mode $L_p = L_J p_p$ and equivalent capacitance $C_p = 1/\omega^2 L_J p_p$. We can construct the imaginary part of the admittance function for the two mode case as

$$ImY(\omega) = \frac{\left(\omega C_1 - \frac{1}{\omega L_1}\right)\left(\omega C_2 - \frac{1}{\omega L_2}\right)}{\left(\omega C_1 - \frac{1}{\omega L_1}\right) + \left(\omega C_2 - \frac{1}{\omega L_2}\right)} \tag{5.28}$$

The zeroes of this function will provide the resonant frequencies. If we take $\omega_1 = 1/\sqrt{L_1 C_1}$ and $\omega_2 = 1/\sqrt{L_2 C_2}$, we see that this is actually the case. Now substituting what we obtained in our analysis, we get the imaginary part of the impedance function as

$$ImY(\omega) = \frac{\left(\frac{\omega}{\omega_1^2} - \frac{1}{\omega}\right)\left(\frac{\omega}{\omega_2^2} - \frac{1}{\omega}\right)}{L_J\omega\left(\frac{p_2}{\omega_1^2} + \frac{p_1}{\omega_2^2}\right) - \frac{L_J}{\omega}} \tag{5.29}$$

5.5 Numerical analysis of a transmon in a 3D cavity

5.5.1 Setting up the system in COMSOL

We construct the transmon in the 3D cavity using the following parameters

Length of cavity	28 mm
Breadth of cavity	28 mm
Height of cavity	28 mm
Substrate thickness	330 μm
Substrate width	4 mm
Substrate length	6 mm
Pad length	500 μm
Pad breadth	250 μm
Inductance length	200 μm
Linear inductance of JJ(L_J)	10 nH

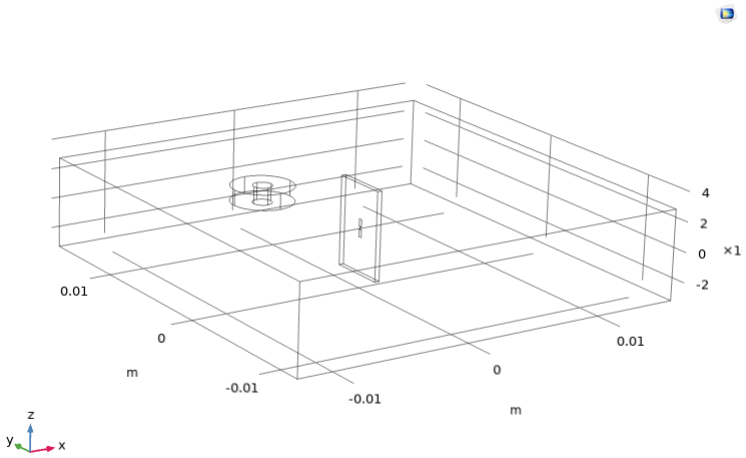

Figure 5.5: Construction of the 3D cavity in COMSOL

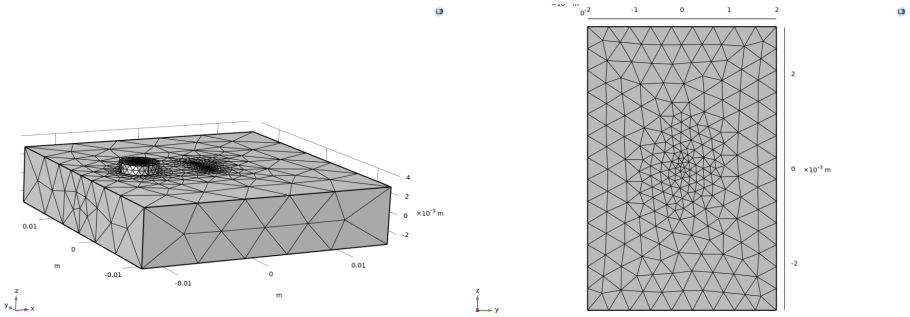

Figure 5.6: Mesh construction of a) the 3-D cavity b) The substrate

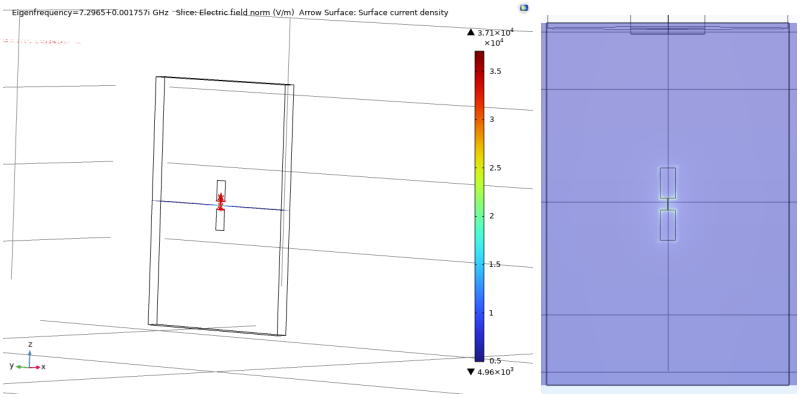

Figure 5.7: Computation results

5.5.2 Chi matrix calculation using EPR

In this case,we change the port of the cavity to the Josephson junction. We run the simulation in COMSOL and we get the following results.

Eigenfrequencies (GHz)	EPR (Method 1)	EPR (Method 2)
5.48+9.40E-6i	0.96038	0.96033
7.30+0.001i	0.010165	0.010164

Here methods 1 and 2 refer to the numerical methods discussed in Section 3.2.2. From the formulas, we get the χ matrix as

$$\chi(GHz) = \begin{bmatrix} -2.11e+02 & -5.97e+00 \\ -5.97e+00 & -4.20e-02 \end{bmatrix} \tag{5.30}$$

5.5.3 Chi matrix calculation using Blackbox quantization

We run the simulation in COMSOL and get the zero crossings at 5.41 GHz and 7.296 GHz. These correspond to the qubit and cavity modes respectively Hence from the theory,

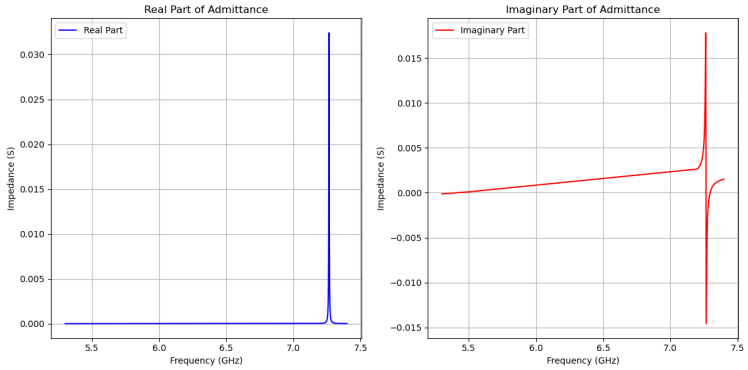

Figure 5.8: Plot of real and imaginary part of admittance with respect to frequency

$$\omega_1 = 5.48GHz \qquad \omega_2 = 7.30GHz$$
$$ImY'(\omega_1) = 1.13217 \times 10^{-12}\Omega^{-1}s^{-1} \qquad ImY'(\omega_2) = 6.24997 \times 10^{-11}\Omega^{-1}s^{-1}$$
$$\implies C_1 = 5.66085 \times 10^{-13}F \qquad C_2 = 3.12498 \times 10^{-11}F$$
$$\implies Q_1 = 309895.25 \qquad Q_2 = 2085.41$$
$$\implies T_1 \text{ for } qubit = 0.05ms \qquad T_1 \text{ for resonator} = 2.8 \times 10^{-4}ms$$

We obtain the matrix χ as

$$\chi = \begin{bmatrix} -2.06e+02 & -5.72e+00 \\ -5.72e+00 & -3.96e-02 \end{bmatrix} \tag{5.31}$$

5.6 Conclusion

In this section, we have performed a detailed analysis of the transmon qubit, using both the techniques of blackbox quantization and EPR. We obtained the Lagrangian of the system, diagonalized it, and obtained the eigenfrequencies. We also obtained the diagonalized Hamiltonian, quantized it and looked at the avoided crossing of eigenvalues. Then we obtained the EPR, and obtained the χ matrix using the same. We tactfully obtained the χ matrix in terms of blackbox quantization, hence establishing a bridge between the blackbox quantization and EPR methods, which became evident when we wrote the impedance function in terms of eigenfrequencies and EPR values. We finally concluded this chapter by numerically computing the same values using COMSOL, and find that χ matrix obtained using both the methods are almost the same.

Chapter 6

Analytical computation of coupled system having opposite anharmonicities

6.1 Hamiltonian of a coupled system having opposite anharmonicities

We take the Hamiltonian

$$H = \frac{p_1^2}{2m_1} + \frac{1}{2}k_1x_1^2 + \frac{p_2^2}{2m_2} + \frac{1}{2}k_2x_2^2 + gx_1x_2 + \alpha x_1^4 - \alpha x_2^4 = \mathcal{H}_0 + V \tag{6.1}$$

We treat the nonlinear terms separately, we first take the term

$$\mathcal{H}_0 = \frac{p_1^2}{2m_1} + \frac{1}{2}k_1x_1^2 + \frac{p_2^2}{2m_2} + \frac{1}{2}k_2x_2^2 + gx_1x_2 \tag{6.2}$$

We shall try diagonalizing the Hamiltonian $\mathcal{H}_0$ first, then we shall treat the perturbation. We write the Hamiltonian in the matrix form

$$\mathcal{H}_0 = \frac{1}{2}P^TM^{-1}P + \frac{1}{2}Q^TKQ, \tag{6.3}$$

where

$$P = \begin{bmatrix} p_1 \\ p_2 \end{bmatrix} \quad Q = \begin{bmatrix} x_1 \\ x_2 \end{bmatrix} \quad M^{-1} = \begin{bmatrix} \frac{1}{m_1} & 0 \\ 0 & \frac{1}{m_2} \end{bmatrix} \quad K = \begin{bmatrix} k_1 & g \\ g & k_2 \end{bmatrix}$$

We can rewrite this as

$$\mathcal{H}_0 = \frac{1}{2}P'^TP' + \frac{1}{2}Q'^TK'Q', \tag{6.4}$$

where

$$P = \begin{bmatrix} \frac{p_1}{\sqrt{m_1}} \\ \frac{p_2}{\sqrt{m_2}} \end{bmatrix} \quad Q = \begin{bmatrix} \sqrt{m_1}x_1 \\ \sqrt{m_2}x_2 \end{bmatrix} \quad K = \begin{bmatrix} \frac{k_1}{m_1} & \frac{g}{\sqrt{m_1m_2}} \\ \frac{g}{\sqrt{m_1m_2}} & \frac{k_2}{m_2} \end{bmatrix}$$

We diagonalize the K' matrix using the rotation matrix

$$RK'R^T = \Omega^2 = \begin{bmatrix} \omega_1^2 & 0 \\ 0 & \omega_2^2 \end{bmatrix}, \tag{6.5}$$

where

$$R = \begin{bmatrix} cos\theta & -sin\theta \\ sin\theta & cos\theta \end{bmatrix} \quad tan2\theta = \frac{\frac{2g}{\sqrt{m_1m_2}}}{\frac{k_1}{m_1} - \frac{k_2}{m_2}}$$

$$\omega_{1,2} = \frac{\frac{k_1}{m_1} + \frac{k_2}{m_2}}{2} \pm \frac{1}{2}\sqrt{\left(\frac{k_1}{m_1} - \frac{k_2}{m_2}\right)^2 + 4\frac{g^2}{m_1m_2}}$$

We can rewrite the matrix as

$$R = \begin{bmatrix} \sqrt{\frac{D+X}{2D}} & -\sqrt{\frac{D-X}{2D}} \\ \sqrt{\frac{D-X}{2D}} & \sqrt{\frac{D+X}{2D}} \end{bmatrix}, \tag{6.6}$$

where

$$D = \sqrt{\left(\frac{k_1}{m_1} - \frac{k_2}{m_2}\right)^2 + \left(\frac{2g}{\sqrt{m_1 m_2}}\right)^2} \qquad X = \frac{k_1}{m_1} - \frac{k_2}{m_2} \qquad Y = \frac{2g}{\sqrt{m_1 m_2}}$$

Now we can write the Hamiltonian in the new basis

$$H = \frac{\tilde{p}_1^2}{2} + \frac{1}{2}\omega_1^2 \tilde{x}_1^2 + \frac{\tilde{p}_2^2}{2} + \frac{1}{2}\omega_2^2 \tilde{x}_2^2 + \alpha \tilde{x}_1^4(x_1, x_2) - \alpha x_2^4(x_1, x_2) = \frac{1}{2}\tilde{P}^T \tilde{P} + \frac{1}{2}\tilde{Q}^T \Omega^2 \tilde{Q} = \mathcal{H}_0 + V, \tag{6.7}$$

where

$$\tilde{P} = RP' \qquad \tilde{Q} = RQ'$$

6.2 Cancellation of nonlinearity for degenerate case

If we take the degenerate case ($k_1 = k_2, m_1 = m_2$) the R matrix simply becomes

$$R = \frac{1}{\sqrt{2}} \begin{bmatrix} 1 & -1 \\ 1 & 1 \end{bmatrix}, \tag{6.8}$$

So $\tilde{P}$ and $\tilde{Q}$ will become

$$\tilde{P} = \frac{1}{\sqrt{2m}} \begin{bmatrix} p_1 - p_2 \\ p_1 + p_2 \end{bmatrix} \qquad \tilde{Q} = \sqrt{\frac{m}{2}} \begin{bmatrix} x_1 - x_2 \\ x_1 + x_2 \end{bmatrix} \tag{6.9}$$

So the Hamiltonian becomes

$$H = \frac{\tilde{p}_1^2}{2} + \frac{1}{2}\omega_1^2 \tilde{x}_1^2 + \frac{\tilde{p}_2^2}{2} + \frac{1}{2}\omega_2^2 \tilde{x}_2^2 + \alpha \left(\frac{m^2}{4}\right)(\tilde{x}_1 + \tilde{x}_2)^4 - \alpha \left(\frac{m^2}{4}\right)(\tilde{x}_1 - \tilde{x}_2)^4 \tag{6.10}$$

Now, simplifying the non-linear terms

$$\begin{aligned} \alpha \left(\frac{m^2}{4}\right)(\tilde{x}_1 + \tilde{x}_2)^4 - \alpha \left(\frac{m^2}{4}\right)(\tilde{x}_1 - \tilde{x}_2)^4 &= \alpha \left(\frac{m^2}{4}\right)[(\tilde{x}_1 + \tilde{x}_2)^4 - (\tilde{x}_1 - \tilde{x}_2)^4] \\ &= \alpha \left(\frac{m^2}{4}\right)[(\tilde{x}_1 + \tilde{x}_2)^2 + (\tilde{x}_1 - \tilde{x}_2)^2][(\tilde{x}_1 + \tilde{x}_2)^2 - (\tilde{x}_1 - \tilde{x}_2)^2] \\ &= \alpha \left(\frac{m^2}{4}\right) 2[\tilde{x}_1^2 + \tilde{x}_2^2][2\tilde{x}_1 \tilde{x}_2] \\ &= \alpha m^2 [\tilde{x}_1^2 + \tilde{x}_2^2][\tilde{x}_1 \tilde{x}_2] \end{aligned} \tag{6.11}$$

Now the Hamiltonian becomes

$$H = \frac{\tilde{p}_1^2}{2} + \frac{1}{2}\omega_1^2 \tilde{x}_1^2 + \frac{\tilde{p}_2^2}{2} + \frac{1}{2}\omega_2^2 \tilde{x}_2^2 + \alpha m^2 [\tilde{x}_1^2 + \tilde{x}_2^2][\tilde{x}_1 \tilde{x}_2] \tag{6.12}$$

Now writing in terms of creation and annihilation operators and removing constant terms

$$H = \hbar\omega_1 a_1^\dagger a_1 + \hbar\omega_2 a_2^\dagger a_2 + \alpha m^2 [(a_1 + a_1^\dagger)^2 + (a_2 + a_2^\dagger)^2][(a_1 + a_1^\dagger)(a_2 + a_2^\dagger)] \tag{6.13}$$

We further expand the nonlinear terms as

$$\begin{aligned} [(a_1 + a_1^\dagger)^2 + (a_2 + a_2^\dagger)^2][(a_1 + a_1^\dagger)(a_2 + a_2^\dagger)] &= [(a_1 + a_1^\dagger)^3 (a_2 + a_2^\dagger) + (a_2 + a_2^\dagger)^3 (a_1 + a_1^\dagger)] \\ &= [a_1^3 + (a_1^\dagger)^3 + 3a_1 a_1^\dagger (a_1 + a_1^\dagger)(a_2 + a_2^\dagger)] \\ &\quad + [a_2^3 + (a_2^\dagger)^3 + 3a_2 a_2^\dagger (a_2 + a_2^\dagger)(a_1 + a_1^\dagger)] \end{aligned} \tag{6.14}$$

For the Hamiltonian to preserve number, there should be a equal number of creation and annihilation operators, but we see none in the nonlinear term, so the nonlinear contribution will be zero, even in the first order perturbation theory.

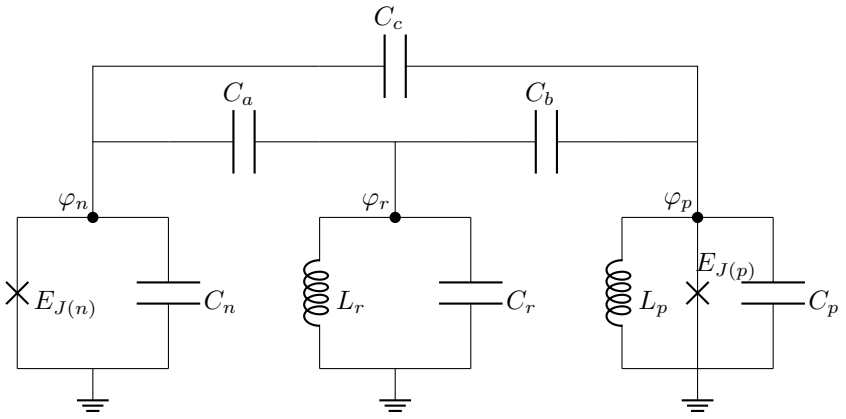

Figure 6.1: A model system to study positive and negative anharmonicity

The Lagrangian of the above circuit can be written as

$$\mathcal{L} = \frac{1}{2}C_n\dot{\varphi}_n^2 + \frac{1}{2}C_r\dot{\varphi}_r^2 + \frac{1}{2}C_p\dot{\varphi}_p^2 + \frac{1}{2}C_a(\dot{\varphi}_n - \dot{\varphi}_r)^2 + \frac{1}{2}C_b(\dot{\varphi}_p - \dot{\varphi}_r)^2 + \frac{1}{2}C_c(\dot{\varphi}_p - \dot{\varphi}_n)^2 \tag{6.15}$$

$$-\frac{1}{2}\frac{\varphi_r^2}{L_r} - \frac{1}{2}\frac{\varphi_p^2}{L_p} - E_{J(n)}cos(\varphi_n) - E_{J(p)}cos(2\pi\frac{\Phi_{ext}}{\phi_0} - \varphi_p) \tag{6.16}$$

or, this can be written in matrix form as

$$\mathcal{L} = \frac{1}{2}\dot{\Phi}_t^T C\dot{\Phi}_t - \frac{1}{2}\Phi_t^T L^{-1}\Phi_t \tag{6.17}$$

where,

$$\dot{\Phi}_t = \begin{bmatrix}\dot{\varphi}_p\\ \dot{\varphi}_n\\ \dot{\varphi}_r\end{bmatrix} \quad C = \begin{bmatrix}C_p + C_b + C_c & C_c & C_b\\ C_c & C_n + C_a + C_c & C_a\\ C_b & C_a & C_r + C_a + C_b\end{bmatrix} \quad L = \begin{bmatrix}L_1 & 0 & 0\\ 0 & L_2 & 0\\ 0 & 0 & L_3\end{bmatrix}$$

and $L_{J(p/n)} = 1/E_{J(p/n)}$ and L_1, L_2 are the equivalent inductances for the positive and negative anharmonic qubits respectively.

We shall follow the same approach as the Transmon case, except for this time, we will obtain three modes owing to the fact that there are three oscillators (One linear and two nonlinear).

We do the similar procedure and we obtain this time the matrix to be diagonalized as

$$M = L^{1/2}CL^{1/2} = \begin{bmatrix}(C_p + C_b + C_c)L_1 & C_c\sqrt{L_1L_2} & C_b\sqrt{L_1L_3}\\ C_c\sqrt{L_1L_2} & (C_n + C_b + C_c)L_2 & C_a\sqrt{L_2L_3}\\ C_b\sqrt{L_1L_3} & C_a\sqrt{L_2L_3} & (C_r + C_b + C_c)L_3\end{bmatrix} = \begin{bmatrix}m_{11} & m_{12} & m_{13}\\ m_{21} & m_{22} & m_{23}\\ m_{31} & m_{32} & m_{33}\end{bmatrix} \tag{6.18}$$

Chapter 7

Conclusions and Future Directions

This thesis aims to explore various techniques used in analyzing superconducting circuits, their basic concept in terms of a trial problem, the relation between them, and various qubit designs. Initially in the second chapter, we studied the theoretical background required for analysis by taking the Duffing oscillator and finding the amplitude frequency curve. This curve manifests itself when we measure the S-parameter of the qubit. We used two methods to solve this system, by Harmonic balance and Secular perturbation, and found the bifurcation of solutions. Then we briefly looked at the Josephson effect and the derivation of the Josephson relations using a phenomenological model. Then we did trial problems to understand the concept of EPR and opposite anharmonicity, respectively.

In chapter three, we studied the tools used for the analysis of qubits, namely, the lumped circuit model, circuit quantization, black box quantization, energy participation ratio and finite element methods. In the fourth chapter, we studied different types of designs of superconducting circuits, starting from transmon, then a qubit with positive anharmonicity, and then finally the flux qubit family.

In the fifth chapter, we applied the tools learned to a simple system, a transmon in a 3D cavity. We obtained the Lagrangian, diagonalized it, and obtained EPR from the unitary matrices. Then we analytically calculated the χ matrix and constructed a bridge between the techniques of EPR and blackbox. Then we set up the system in COMSOL and calculate the quantities numerically. In the sixth chapter, we take the case of qubits with opposite anharmonicity and found out if the nonlinear coefficients are same, then the first order perturbation is zero. We also tried a model system like the one for transmon and tried calculating the similar parameters.

For the future directions, some more work can be done in developing a qubit having components of opposite anharmonicity, by designing an equivalent circuit that can be fabricated in the lab. Analytically, we can use the results by Solgun et. al [21] which provides an easy way to obtain impedance functions, provided the qubit is of low anharmonicity and in dispersive limit. Efforts can also be made, in writing a general formula connecting impedance matrix to the EPR ratios, as done in section 5.4.

Bibliography

[1] S M Girvin. Circuit QED: superconducting qubits coupled to microwave photons. In *Quantum Machines: Measurement and Control of Engineered Quantum Systems*, pages 113–256. Oxford University PressOxford, June 2014.

[2] Simon E. Nigg, Hanhee Paik, Brian Vlastakis, Gerhard Kirchmair, S. Shankar, Luigi Frunzio, M. H. Devoret, R. J. Schoelkopf, and S. M. Girvin. Black-box superconducting circuit quantization. *Physical Review Letters*, 108, 2012.

[3] Lev Davidovich Landau and E. M. Lifshitz. *Mechanics*. Butterworth-Heinemann, Elsevier, 1969.

[4] Ali H. Nayfeh and Dean T. Mook. *Nonlinear Oscillations*, chapter 2, pages 39–94. John Wiley & Sons, Ltd, 1995.

[5] Ron Lifshitz and M C Cross. Nonlinear dynamics of nanomechanical resonators. In *Nonlinear Dynamics of Nanosystems*, pages 221–266. Wiley-VCH Verlag GmbH & Co. KGaA, Weinheim, Germany, September 2010.

[6] B D Josephson. Possible new effects in superconductive tunnelling. *Phys. Lett.*, 1(7):251–253, July 1962.

[7] Michel H. Devoret, John M. Martinis, and John Clarke. Measurements of macroscopic quantum tunneling out of the zero-voltage state of a current-biased josephson junction. *Phys. Rev. Lett.*, 55:1908–1911, Oct 1985.

[8] Alexandre Blais, Arne L Grimsmo, S M Girvin, and Andreas Wallraff. Circuit quantum electrodynamics. *Rev. Mod. Phys.*, 93(2), May 2021.

[9] M. H. Devoret. Quantum Fluctuations in Electrical Circuits. In S. Reynaud, E. Giacobino, and J. Zinn-Justin, editors, *Fluctuations Quantiques/Quantum Fluctuations*, page 351, January 1997.

[10] Zlatko K. Minev, Zaki Leghtas, Shantanu O. Mundhada, Lysander Christakis, Ioan M. Pop, and Michel H. Devoret. Energy-participation quantization of josephson circuits. *npj Quantum Information*, 7, 2021.

[11] Ke-Hui Yu, Xiao-Yang Jiao, and Li-Jing Jin. Using the inductive-energy participation ratio to characterize a superconducting quantum chip. *Physical Review Applied*, 21(3), March 2024.

[12] COMSOL Documentation.

[13] H. M. Antia. *Numerical methods for scientists and Engineers*. Hindustan, 2012.

[14] Jens Koch, Terri M Yu, Jay Gambetta, A A Houck, D I Schuster, J Majer, Alexandre Blais, M H Devoret, S M Girvin, and R J Schoelkopf. Charge-insensitive qubit design derived from the cooper pair box. *Phys. Rev. A*, 76(4), October 2007.

[15] Jaseung Ku, Xuexin Xu, Markus Brink, David C McKay, Jared B Hertzberg, Mohammad H Ansari, and B L T Plourde. Suppression of unwanted ZZ interactions in a hybrid two-qubit system. *Phys. Rev. Lett.*, 125(20):200504, November 2020.

[16] Peng Zhao, Peng Xu, Dong Lan, Ji Chu, Xinsheng Tan, Haifeng Yu, and Yang Yu. High-contrast ZZ interaction using superconducting qubits with opposite-sign anharmonicity. *Phys. Rev. Lett.*, 125(20):200503, November 2020.

[17] J R Friedman, V Patel, V, W Chen, S K Tolpygo, and J E Lukens. Quantum superposition of distinct macroscopic states. *Nature*, 406(6791):43–46, July 2000.

[18] Arvind Mamgain, Siddhi Satish Khaire, Ujjawal Singhal, Irshad Ahmad, Lipi Arvindbhai Patel, Kunal Dhanraj Helambe, Sourav Majumder, Vibhor Singh, and Baladitya Suri. A review of developments in superconducting quantum processors. *J Indian Inst Sci*, 103(2):633–669, April 2023.

[19] J Q You, Xuedong Hu, S Ashhab, and Franco Nori. Low-decoherence flux qubit. *Phys. Rev. B Condens. Matter Mater. Phys.*, 75(14), April 2007.

[20] Eric Hyyppä, Suman Kundu, Chun Fai Chan, András Gunyhó, Juho Hotari, David Janzso, Kristinn Juliusson, Olavi Kiuru, Janne Kotilahti, Alessandro Landra, Wei Liu, Fabian Marxer, Akseli Mäkinen, Jean-Luc Orgiazzi, Mario Palma, Mykhailo Savytskyi, Francesca Tosto, Jani Tuorila, Vasilii Vadimov, Tianyi Li, Caspar Ockeloen-Korppi, Johannes Heinsoo, Kuan Yen Tan, Juha Hassel, and Mikko Möttönen. Unimon qubit. *Nat. Commun.*, 13(1):6895, November 2022.

[21] Firat Solgun, David P. DiVincenzo, and Jay M. Gambetta. Simple impedance response formulas for the dispersive interaction rates in the effective hamiltonians of low anharmonicity superconducting qubits. *IEEE Transactions on Microwave Theory and Techniques*, 67(3):928–948, 2019.